Mon. Not. R. Astron. Soc. **000**, 000–000 (1996) Printed 16 January 2014 (MN LATEX style file v1.4)

Formation and Evolution of Elliptical Galaxies and QSO Activity

Amancio C. S. Friaça[1] and Roberto J. Terlevich[2]
[1]*Instituto Astronômico e Geofísico, USP, Av. Miguel Stefano 4200, 04301-904 São Paulo, SP, Brazil*
[2]*Royal Greenwich Observatory, Madingley Road, Cambridge CB3 0EZ, UK*

16 January 2014

ABSTRACT
We present the results of a numerical code that combines multi-zone chemical evolution with 1-D hydrodynamics to follow in detail the evolution and radial behaviour of gas and stars during the formation of elliptical galaxies. We use the model to explore the links between the evolution and formation of elliptical galaxies and QSO activity. The knowledge of the radial gas flows in the galaxy allows us to trace metallicity gradients, and, in particular, the formation of a high-metallicity core in ellipticals. The high-metallicity core is formed soon enough to explain the metal abundances inferred in high-redshift quasars. The star formation rate and the subsequent feedback regulate the episodes of wind, outflow, and cooling flow, thus affecting the recycling of the gas and the chemical enrichment of the intergalactic medium. The evolution of the galaxy shows several stages, some of which are characterized by a complex flow pattern, with inflow in some regions and outflow in other regions. All models, however, exhibit during their late evolution a galactic wind at the outer boundary and, during their early evolution, an inflow towards the galaxy nucleus. The characteristics of the inner inflow could explain the bolometric luminosity of a quasar lodged at the galaxy centre as well as the evolution of the optical luminosity of quasars.

Key words: galaxies: elliptical – galaxies: evolution – galaxies: formation – galaxies: ISM – intergalactic medium – quasars: general

1 INTRODUCTION

Imaging studies of the faint extensions around QSOs indicate that elliptical galaxies are the host galaxies of the radio-loud and the brightest QSOs (Smith et al. 1986; Hutchings, Janson & Neff 1989; Hutchings et al. 1994; Hutchings & Morris 1995; McLeod & Rieke 1995; Aretxaga, Boyle & Terlevich 1995; Disney et al. 1995; Bahcall, Kirkakos & Schneider 1996; Ronnback et al. 1996; Taylor et al. 1996). As a matter of fact, at high redshifts ($z > 2$), the only galactic systems available to harbour QSOs are the spheroids, since the disks are formed much later. In addition, the epoch of completion of the large spheroids ($z > 2$) coincides with the peak in the QSO activity ($2 < z < 3$) (Schmidt et al. 1991), suggesting a relation between the QSO phenomenon and the formation of large ellipticals. In fact, in recent years there has been increasing evidence linking QSO activity with galaxy formation. The high metal content of high redshift QSOs, the high dust content (several 10^8 $M_\odot$ of dust) of distant QSOs (Andreani, Franca & Cristiani 1993; Isaak et al. 1994; McMahon et al. 1994; Omont et al. 1996) plus the possible relation between the galaxy luminosity function (LF) and the QSO LF (Terlevich & Boyle 1993, hereafter TB93; Boyle & Terlevich 1998, hereafter BT98) provides tantalising evidence of this link. In any case, the fact that even the highest redshift QSO has strong metal lines in its spectrum requires that the broad line region (BLR) gas has been enriched by a stellar population formed before $z \sim 5$. Work by TB93 and Hamann & Ferland (1993) (hereafter HF93) highlighted the importance of metal production in the early evolution of a galaxy. Since QSOs are seen up to redshifts of $z \sim 5$, the supersolar metallicities required by the BLR models should be reached by ~ 1 Gyr since the beginning of the galaxy formation epoch. This evolutionary time scale is an important constraint in chemical enrichment models.

Two fundamental relations involving intrinsic parameters of elliptical galaxies show remarkable little dispersion and point towards an early formation of ellipticals. They are the colour-luminosity relation and the "fundamental plane" relating the total luminosity of an elliptical to its central velocity dispersion and surface brightness. The tightness of the colour-luminosity relation provides strong evidence that most of the present stellar population was formed at $z > 2$ (Bower, Lucey and Ellis 1992). The narrowness of the "fundamental plane" gives additional support to that conclusion (Renzini and Ciotti 1993) and in addition indicates that the properties of the core (velocity dispersion, Mg_2 strength) are intimately linked to the galaxy global ones (D_n, luminosity). There is also good evidence that the stellar population in massive ellipticals is metal rich with respect to the Sun, and shows large radial metallicity gradients (e.g., Worthey, Faber and Gonzalez, 1992; Davies, Sadler and Peletier 1993). These properties of the elliptical galaxies may also be related to the fact that they probably harbour QSOs in their centres at some stage of their evolution.

One-zone chemical evolution models have been used (Hamann & Ferland 1992, HF93, Padovani & Matteucci 1993, Matteucci & Padovani 1993) to investigate the chemical history and the fueling of QSOs. However, during the early evolution of the elliptical galaxy, it is expected several episodes of gas outflow and inflow which cannot be followed by the one-zone model. In addition, the one-zone chemical evolution models that attempt to explain the high metal content in high redshift QSOs tend to overproduce metals (averaged over the entire galaxy) and predict an excessively high luminosity for the parent galaxy of the QSO. For example, HF93 model M4 reproduces the rapid metal production needed but it is overluminous. In this model, an elliptical of 10^{11} $M_\odot$ has a peak bolometric luminosity of $\sim 2\times10^{13}$ $L_\odot$ at an age of $\sim$ 0.1 Gyr. But an elliptical with 10^{11} $M_\odot$ is at present only a sub-L^* galaxy (with a blue luminosity of $\sim 0.3L^*$, for $M_B^* = -21$ and $[M/L_B] = 10$), so that for the most luminous ($M_B \approx -24$) ellipticals in the nearby Universe HF93 model M4 predicts luminosities of up to 10^{15} $L_\odot$ during its formation. These luminosities are higher than the QSO luminosities!!

Note that only the core of the galaxy has to be metal rich in accordance with the observed metallicity gradients in nearby galaxies. In the starburst model for QSOs (TB93 and references therein), the QSOs are the young cores of massive ellipticals forming most of the dominant metal-rich population in a short starburst. The core mass, which participates in the starburst, comprises only a small fraction ($\sim$ 5 %) of the total galaxy mass. Also in the standard supermassive black hole model for QSOs, only $0.5-1$ per cent of the galaxy mass goes into the black hole (Haehnelt & Rees 1993). The excessive production of energy and metals in the one-zone model arises, therefore, from its inability to resolve the core of the galaxy.

The QSO LF undergoes strong evolution between $z = 2$ and the present epoch, with the redshift dependence of the LF being well-described by a constant comoving space density and a pure power-law luminosity evolution $L(z) \propto (1+z)^k$ (Boyle et al. 1988, 1991, BT98), with k in the range $3.1 < k < 3.6$. This luminosity evolution is linked to the mass flow into the galactic nucleus hosting the QSO, both in the supermassive black hole scenario and in the starburst model for AGN. Since the luminosity is expected to be proportional to the mass accretion rate into the nucleus, in order to make predictions about the luminosity evolution of the QSO one needs the evolution of the central gas inflow. Again, this piece of information is not provided by the one-zone model.

In view of the limitations of one-zone chemical models, we have developed a multi-zone chemo-dynamical model that self-consistently combines chemical evolution and numerical hydrodynamics. In this paper, we use this code to investigate a number of topics related to formation and evolution of elliptical galaxies and the link young ellipticals-QSOs: 1) the formation of a high-metallicity core in ellipticals; 2) the radial metallicity gradients in ellipticals; 3) the chemical enrichment of the intracluster medium by ellipticals; 4) the evolution of the luminosity of young cores of ellipticals/QSOs. The approach of the present work is first to develop a realistic sequence of models which reproduces the main properties of elliptical galaxies. We then investigate the evolution of the galaxy core and of the gas inflow into the nucleus and, within the scenario in which the galaxy nucleus hosts a QSO, we compare the predictions of the model with QSO observations.

The chemo-dynamical evolution code is described in Section 2. Section 3 presents the evolution of the interstellar medium (ISM) and of the star formation. Section 4 considers the chemical enrichment of the intracluster medium by galactic winds from elliptical galaxies. Section 5 is devoted to abundances and metallicity gradients of the stellar population in ellipticals. The predictions of our models for the evolution of the QSO LF are presented in Section 6. Some concluding remarks are given in Section 7.

2 THE CHEMO-DYNAMICAL MODEL

Apart from spectral-synthesis models not discussed in this paper, two classic approaches have been used to study the formation and evolution of elliptical galaxies: hydrodynamical models aimed at reproducing the evolution of the X-ray emitting gas in elliptical galaxies (David et al. 1990,1991; Ciotti et al. 1991); and one-zone chemical evolution models, which seek to reproduce the global evolution of gas and stars, giving results on the evolution of metal abundances (Arimoto & Yoshii 1987, Matteucci & Tornambé 1987, Padovani & Matteucci 1993, Matteucci & Padovani 1993).

Unfortunately, both models give only a restricted description of the first few Gyrs of the elliptical galaxy, the stage we regard as more interesting in connection to the elliptical galaxies-QSOs link. In the case of the above hydrodynamical models, one central problem is that the gas or ISM represents a major component of the young galaxy, which not only reacts to the input of energy of stars but also, via star formation, builds up the stellar population. Moreover, the deposition of energy, mass and metals into the ISM results from former star generations, and thus in a complete computation of the stellar input into the gas the whole star formation history should be stored.

Regarding the one-zone chemical evolution models, they do not follow the dynamical evolution of the gas, and, in particular, the evolution of the galactic wind, a central ingredient in many of these models. The gas distribution and velocity field are not described by these models, since the situation is far more complex than the existence or not of a galactic wind. The gas flow is not necessarily coordinated along the galaxy; there could be inflow at one radius and outflow at another radius. In addition, these models do not give information on the space distribution of the stars formed and metallicity gradients. This latter issue is needed for the understanding of the evolution of the core of the ellipticals, the region which is most readily observable, where the metal-rich stars are located, and which lodges the QSO.

A more promising approach is represented by the chemo-dynamical model, which combines hydrodynamical and chemical evolution. Such models have been employed to study elliptical galaxies (Burkert & Hensler 1989; Theis, Burkert & Hensler 1992) and spiral galaxies (Burkert, Truran & Hensler 1992; Samland, Hensler & Theis 1997). The chemo-dynamical model avoids a number of uncertainties of the one-zone models. One common assumption, for example, is that star formation ceases after the system has evolved long enough. For instance, in HF93 models, star formation stops when the gas mass fraction drops below 3%. This in principle recognizes the existence of a density threshold for star formation (Kennicutt 1989), but the choice of the value of the critical density (or gas fraction) is arbitrary. On the other hand, Matteucci & Padovani (1993) models assume, as most of the chemical evolution models do, that the star formation stops when the galactic wind starts. The existence of galactic winds in ellipticals was first suggested by Mathews & Baker (1971) in order to explain the apparent lack of gas in these systems. Later, Larson (1974b) invoked galactic winds to reproduce the relation mass-metallicity in ellipticals. Following Larson, the condition for the onset of a galactic wind in Matteucci & Padovani (1993) models is that the thermal energy content of the gas heated by SNe exceeds the binding energy of the gas. Note, however, that the suppression of star formation by galactic winds assumes that the wind instantly devoids the galaxy of gas. A more realistic approach should include the time delay due to the finite flow velocity of the gas leaving the galaxy. Moreover, winds will not necessarily curtail all star formation, as can be seen from observations of starburst galaxies which can have simultaneously kpc-scale X-ray wind and ongoing massive star formation (Heckman, Armus & Miley 1987).

In the present work we use the chemo-dynamical model developed by Friaça & Terlevich (1994) to follow the evolution of elliptical galaxies from the protogalaxy stage. The model combines a multi-zone chemical evolution solver and a 1-D hydrodynamical code. The elliptical galaxy, assumed to be spherical, is subdivided into several spherical zones and the hydrodynamical evolution of its ISM is calculated (see Friaça 1986, 1990, 1993). Then, taking into account the gas flow, the chemical evolution equations are solved for each zone. In this work, 100 zones are used, with the inner boundary at 100 pc and the outer boundary at the galaxy tidal radius. A total of $\approx$ 100 star generations over 13 Gyr is stored for the chemical evolution calculations. The length of the star generations increases with the stellar age, ranging from 10^6 yr for newly formed stars to $\approx 3 \times 10^8$ yr for the oldest stars. Our models include inhibition of star formation when the density is too low or when the gas is expanding, but the star formation is never sharply cut off and continues after the first galactic wind has been established. This allows us to study the whole star formation history of the galaxy, as well as the development of both late wind and late cooling flow episodes.

2.1 The hydrodynamical evolution

The hydrodynamical evolution of the spherically symmetric ISM is given by solving the fluid equations of mass, momentum and energy conservation

$$\frac{\partial \rho}{\partial t} + \frac{1}{r^2}\frac{\partial}{\partial r}(r^2 \rho u) = \alpha \rho_* - \nu \rho, \tag{1}$$

$$\frac{\partial u}{\partial t} + u\frac{\partial u}{\partial r} = -\frac{1}{\rho}\frac{\partial p}{\partial r} - \frac{GM}{r^2} - \alpha\frac{\rho_*}{\rho}u, \tag{2}$$

$$\begin{aligned}\frac{\partial U}{\partial t} + u\frac{\partial U}{\partial r} \quad = \quad & \frac{p}{\rho^2}\left(\frac{\partial \rho}{\partial t} + u\frac{\partial \rho}{\partial r}\right) - \Lambda\rho \\ & + \alpha\frac{\rho_*}{\rho}\left(U_{inj} + \frac{u^2}{2} - U - \frac{p}{\rho}\right),\end{aligned} \tag{3}$$

where ρ, u, p, and U are the gas density, velocity, pressure and specific internal energy. The equation of state $U = (3/2)p/\rho$ completes the system of equations. The total binding mass M is the sum of three components: gas, stars and a dark halo, M_g, M_*, M_h, respectively. The gas and the stars exchange mass through star formation and stellar mass losses (supernovae, planetary nebulae, and stellar winds). The dark halo has no interplay with the gas and the stars, and it is given by a static mass density distribution $\rho_h(r) = \rho_{h0}[1+(r/r_h)^2]^{-1}$, where ρ_{h0} is the halo central density and r_h is the halo core radius.

The star formation process and the restoring of mass to the ISM by dying stars are represented by the specific rates for star formation ν and for gas return α. The terms $\alpha\rho_*$ and $\nu\rho$ in the continuity equation couple the gas density to the stellar mass density ρ_*. It is expected that the stars do not remain in the zones in which they are formed. In addition, the final positions to where they have moved should reproduce the density profile of a realistic galaxy. We take this into account by radially moving each zone of newly formed stars in one free-fall time to a final position such as the resulting stellar mass distribution follows a King profile $\rho_*(r) = \rho_{*0}[1 + (r/r_c)^2]^{-3/2}$, where ρ_{*0} and r_* are the central stellar density and the stellar core radius, respectively. Both the stellar distribution and the dark halo are truncated at a common tidal radius r_t, beyond which there is no star formation.

The stars are assumed to die either as supernovae (SNe) or as planetary nebulae, when instantaneous ejection of mass and energy occurs. The energy per unit mass injected into the gas by the dying stars can be divided in three contributions due to Type I SNe, Type II SNe and quiescent stellar mass loss (planetary nebulae and stellar winds)

$$\begin{aligned}U_{inj} \quad = \quad & (\alpha_{SNI}E_{SNI}/M_{SNI} + \alpha_{SNII}E_{SNII}/M_{SNII} \\ & + \alpha_* U_{inj,*})/\alpha,\end{aligned} \tag{4}$$

where α_{SNI}, α_{SNII}, and α_* are the specific gas return rate by Type I SNe, Type II SNe, and quiescent stellar mass loss, respectively ($\alpha = \alpha_{SNI} + \alpha_{SNII} + \alpha_*$). M_{SNI} and M_{SNII}, E_{SNI} and E_{SNII} are the mass and kinetic energy of the supernova ejecta, respectively. Here, Type I SN stands for Type Ia only, whereas Type Ib is included in the Type II SN. The gas which is lost from stars as wind or planetary nebulae is assumed to be thermalized to the temperature given by the velocity dispersion of the stars (i.e., $U_{inj,*} = (3/2)\sigma_*^2$, where σ_* is the one-dimensional stellar velocity dispersion).

The adopted cooling function $\Lambda(T)$, defined so that $\Lambda(T)\rho^2$ is the cooling rate per unit volume, takes into account the variations of the gas abundances predicted by the chemical evolution calculation. For the sake of simplicity, instead of considering the abundances of all elements included in the chemical evolution calculations, our cooling function depends only the abundances of O and Fe, which are the main coolants for $T > 10^5$ K. In the evaluation of the cooling function, the abundances of elements other than Fe and O have been scaled to the O abundance as $y_i = y_{i,P} + (y_{i,\odot} - y_{i,P}) y_O / y_{O,\odot}$, where y_i is the abundance by number of the element i (the cooling function takes into account emission from H, He, C, N, O, Ne, Mg, Si, S, Cl, Ar and Fe), and $y_{i,P}$ and $y_{i,\odot}$ are the primordial (i.e., Y=0.24 and Z=0.0) and solar (Grevesse & Anders 1989) abundances of the element i. The atomic database used in the determination of the cooling function comes from the photoionization code AANGABA (Gruenwald & Viegas 1992). A novelty of these models is the self-consistency of the hydrodynamics, chemical evolution and atomic physics, since the cooling function is evaluated based on the actual chemical abundances obtained from the chemo-dynamical modelling.

The spherically symmetric hydrodynamics equations are solved using a finite-difference, implicit code based on Cloutman (1980). The code is run in the Euleurian mode and the grid points are spaced logarithmically. The grid has between 150 and 300 cells, the first cell being 50 pc wide. The innermost cell edge is located at 100 pc and the outer boundary at twice the tidal radius of the galaxy. The artificial viscosity for the treatment of the shocks follows the formulation of Tsharnutter & Winkler (1979) based on the Navier-Stokes equation. In contrast with the von Neumann–Richtmyer artificial viscosity (Richtmyer & Morton 1967), this form of artificial viscosity vanishes for an homologous contraction.

The outer boundary conditions on pressure and density are derived by including an outer fictitious cell, the density and pressure in which are obtained from extrapolation of power laws over the radius fitted to the five outermost real cells. The inner boundary conditions adjust according to whether inflow or outflow prevails locally. During inflow, the velocity at the inner boundary is extrapolated from the velocities at the innermost cell edges whereas during outflow, the velocity at the inner boundary is set to zero.

The initial conditions assume an entirely gaseous ($M_* = 0$) protogalaxy. The gas has temperature $T_0 = 10^4$ K, primordial chemical abundances and density distribution following that of the dark halo. The models are evolved until the present epoch ($t_G = 13$ Gyr). A $H_0 = 50$ km s^{-1} Mpc^{-1}, $\Omega = 1$ cosmology is adopted throughout this paper.

2.2 The chemical evolution

Chemical evolution occurs as stars form out of the ISM evolve and eject gas back into the ISM via stellar winds, planetary nebulae and SNe. In this work, we use conventional chemical evolution formulations frequently used in classic one-zone models in order to make it easier comparison with previous works. Within each spherical zone, in which the model galaxy has been divided, the evolution of the abundances of six chemical species (He, C, N, O, Mg, Fe) is calculated by solving the basic equations of chemical evolution (Talbot & Arnett 1973, Tinsley 1980, Matteucci & Tornambè 1987). We do not assume instantaneous recycling approximation for the chemical enrichment, but instead the delays for gas restoring from the stars are taken into account by using main-sequence lifetimes t_m (in Gyr) $\log m = 0.0558 \log^2 t_m - 1.338 \log t_m + 7.764$ for stellar masses $m \leq 6.6\,\mathrm{M}_\odot$ (Renzini & Buzzoni 1986), and $t_m = 1.2 m^{-1.85} + 0.003$ for $m > 6.6\,\mathrm{M}_\odot$ (Güsten & Mezger 1983). Instantaneous mixing with the ISM is assumed for the stellar ejecta.

We express the relation of the star formation rate (SFR) to the gas content, by writing the SFR as $\psi(r,t) = \nu\rho$, where ν is the specific SFR. Unfortunately, there is no widely accepted theory of star formation. Thus, following Schmidt (1959, 1963), one usually adopts a dependency of ν on a power of the gas density,

$$\nu = \nu_0 (\rho/\rho_0)^{n_{SF}}. \tag{5}$$

$n_{SF} = 0$ and $n_{SF} = 1$ for the linear ($\psi \propto \rho$) and the quadratic ($\psi \propto \rho^2$) models of Schmidt. It is not expected that the SFR strictly follows a power law of the density; the parameter n_{SF} is meant only to describe the nonlinearity of the dependence of the SFR on the gas content. There are, however, good theoretical and observational reasons for believing that the SFR depends at least linearly on the gas content. Kennicutt (1989) finds that the SFR per unit area of disk galaxies varies approximately as the 1.3 power of the gas surface density. Chemical evolution models for the Galaxy require a weak dependence of the SFR on the gas density: a range $n_{SF} = 0 - 0.5$ is found by Rana & Wilkinson (1986), whereas Matteucci & François (1989) favor $n_{SF} = 0.1$ over $n_{SF} = 1$. Some values of n_{SF} suggested for idealized cases bracket the observational estimates above. In this paper, most of the models have the so-called *standard SFR*, i.e., $n_{SF} = 1/2$, in which the time scale for star formation is proportional to the local dynamical time (Larson 1974a). Models have also been run for a $n_{SF} = 1/3$ SFR, which corresponds to a cloud collision model for star formation with constant filling factor of the star-forming clouds (Negroponte & White 1983), and a linear SFR ($n_{SF} = 0$) (the simplest case). The normalization in eq. (5) was set as $\nu_0 = 10$ Gyr^{-1} in agreement with the $\sim 10^8$ yr time scale for star formation required by chemical evolution models in order to reproduce the supersolar [Mg/Fe] ratio in giant ellipticals (Matteucci & Tornambé 1987; Matteucci 1992). The fiducial value for the gas density ρ_0 is taken as the initial average gas density inside the halo core radius. We included inhibition of star formation for expanding gas ($\nabla.u > 0$) or inefficient cooling (i.e., for a cooling time $t_{coo} = (3/2) k_B T / \mu m_H \Lambda(T) \rho$ is longer than the dynamical time $t_{dyn} = (3\pi/16\,G\,\rho)^{1/2}$) by multiplying ν as defined in eq. (5) by the inhibition factors $(1 + t_{dyn} \max(0, \nabla.u))^{-1}$ and $(1 + t_{coo}/t_{dyn})^{-1}$.

The stellar birthrate (per unit volume) of stars of mass m is given by $\psi(r,t)\phi(m)$, where $\phi(m)$ is the initial mass function by number (IMF). The IMF is assumed to be independent on time and position and given by $\phi(m) = C\, m^{(1+x)}$. Here we adopt a Salpeter IMF ($x = 1.35$), normalized over the mass range $m = 0.1 - 100$ M$_\odot$.

The gas restoring from the stars depends on the initial stellar mass. Single stars in the mass range $0.1 < m/\,\mathrm{M}_\odot < 8$ end their life as planetary nebulae and leave helium or C-O white dwarfs with masses smaller than 1.4 M$_\odot$. Single stars with masses above 8 M$_\odot$ end their life as Type II SNe. No distinction is made between Type II and Type Ib, Type Ib being considered a Type II which has lost its envelope prior to the explosion. Type Ia supernovae are assumed to originate from binary systems of total mass in the range $3 < m/\,\mathrm{M}_\odot < 16$ in which the primary evolves until it becomes a C-O white dwarf. Mass transfer from the slower-evolving secondary triggers C-deflagration onto the primary when the latter reaches the Chandrasekhar mass (Whelan & Iben 1973). The computation of the Type Ia SN rate follows Greggio & Renzini (1983). An important parameter in this scenario is $A_{SN\,I}$, the mass fraction of the IMF between $3 < m/\mathrm{M}_{\odot} < 16$ that goes to binary systems giving rise to Type Ia SNe. Following Matteucci & Tornambé (1987) and Matteucci (1992), we have chosen $A_{SN\,I} = 0.1$. This value should be verified *a posteriori* by checking the predicted against the observed SN Ia rate in ellipticals.

The nucleosynthesis prescriptions for the envelopes of single intermediate mass stars ($0.8 < m/\mathrm{M}_{\odot} < 8$) are taken from Renzini & Voli (1981) (their case with $\alpha_c = 0$, $\eta = 0.33$). We consider production of secondary N via CNO shell burning in the envelopes of massive stars ($m > 8\ \mathrm{M}_{\odot}$) following the case B of Talbot & Arnett (1973) (100% conversion of the envelope C and O into N). For stars in the mass range $8-10\,\mathrm{M}_{\odot}$, the nucleosynthesis prescriptions are those suggested by Hillebrandt (1982,1985). The yields from Type II SNe with progenitors with mass between 10 and 40 $\mathrm{M}_{\odot}$ are from Weaver & Woosley (1993) and Woosley & Weaver (1995), using a value of the $^{12}C(\alpha,\gamma)^{16}O$ reaction rate which is 1.7 times the Caughlan & Fowler (1988) value. The results from the nucleosynthesis calculations for stars more massive than $\approx 18\ \mathrm{M}_{\odot}$ depend critically on the chosen value of this reaction rate. Since Woosley & Weaver (1995) do not calculate models for SN II progenitors more massive than 40 $\mathrm{M}_{\odot}$, we extrapolate their yields for the mass range 40-100 $\mathrm{M}_{\odot}$ based on the trend of yields with increasing mass derived from Woosley & Weaver (1986), who use a higher value for the $^{12}C(\alpha,\gamma)^{16}O$ reaction rate. For masses above 30 $\mathrm{M}_{\odot}$, the results also depend on the assumed kinetic energy at infinite KE_{∞} of the piston of the explosion. If KE_{∞} is not large enough, there is some fall-back of material, and a more massive remnant (a black hole) is formed, locking the nucleosynthesis products and reducing the yields, specially that of the iron. Larger values of KE_{∞} prevent the fall-back and lead to a larger amount of ejected iron. The sequence A of models of Woosley & Weaver has nearly constant KE_{∞}, so that fall-back is not prevented, a black hole is formed and little iron is ejected. In this work, we use the sequence with KE_{∞} increasing with mass (models S30B, S35C and S40C), resulting in larger Fe yields and smaller remnants. Finally, the yields from Type Ia SNe are from Nomoto et al. (1984) (their model W7).

We adopt the initial mass–final mass relation given by Iben & Renzini (1983) for the white dwarf remnants of single stars with initial mass in the range $0.1 < m/\mathrm{M}_{\odot} < 8$. Stars more massive than 8 $\mathrm{M}_{\odot}$, which explode as Type II (or Ib) supernovae are assumed to leave 1.4 $\mathrm{M}_{\odot}$ neutron stars remnants. The Type Ia supernovae are assumed to leave no remnant.

We performed several checks of the chemical evolution solver of our code by comparing the results of one-zone runs with classic galactic wind one-zone models for elliptical galaxies (Arimoto & Yoshii 1987, Matteucci & Tornambé 1987, Matteucci 1992). Here we consider a reference one-zone model, similar to the model A2 of Matteucci (1992), except for some differences in the nucleosynthesis prescriptions and stellar lifetimes. Our model represents a galaxy initially gaseous with mass $M_G = 10^{12}\ \mathrm{M}_{\odot}$, and no dark halo. It is assumed a linear star formation law, i.e. $\nu_{SF} = \nu_0 =$ constant. Following the relation $\nu = 8.6(M_G/10^{12}\ \mathrm{M}_{\odot})^{-0.115}$ Gyr^{-1} derived by Arimoto & Yoshii (1987), ν_0 is set as 9 Gyr^{-1}. The model belongs to the class of SN-driven galactic wind models, in which a galactic wind is established at a time t_{gw}. At this time, the gas is swept from the galaxy and the star formation is turned off forever. The condition for the onset of the galactic wind is that the thermal content of the SN remnants of the galaxy equals the gravitational binding energy of the galaxy ISM (the computation of these two quantities follows Matteucci 1992). Our model gives $t_{gw} = 0.81$ Gyr, in good agreement with $t_{gw} = 1.01$ Gyr of model A2 of Matteucci (1992).

Figure 1. The evolution of abundance ratios for our reference one-zone model illustrating the effect of the convection parameter α_c of the models of Renzini & Voli (1981) for the yieds of intermediate mass stars. Throughout this paper, the bracketed ratios denote the ratio of mass abundances relative to their solar values.

Fig. 1 shows the evolution of abundances of C, N, O, Mg and Fe for our reference model. Our results for the abundance evolution are similar to those of the model M4 of HF93 and the model of Matteucci & Padovani (1993) with luminous mass of $10^{12}\ \mathrm{M}_{\odot}$ and Salpeter IMF (note that HF93 assumes $\nu_0 = 6.7$ Gyr^{-1} and $x = 1.1$ for the IMF, and Matteucci & Padovani model includes a dark halo). In order to illustrate the effect of the convection parameter α_c of the models of Renzini & Voli (1981) for the yields of intermediate mass stars, we show runs for their cases ($\alpha_c = 0$, $\eta = 0.33$) and ($\alpha_c = 1.5$, $\eta = 0.33$). The effect of α_c can be seen in the evolution of [N/H] (throughout this paper, the bracketed ratios denote the ratio of mass abundances relative to their solar values, i.e., $[\mathrm{X/H}] \equiv (\mathrm{X/H})/(\mathrm{X/H})_{\odot}$). For $\alpha_c = 0$, there is secondary only N production, and for $\alpha_c = 1.5$ there is some primary production of N due to hot-bottom burning in the stellar envelope. Earlier than 3×10^7 yr, there is only secondary production of N by high mass stars and the pace of N enrichment is roughly proportional to the gas metallicity. For later times, the yield of stars with $m < 8\ \mathrm{M}_{\odot}$ is important, and in the case $\alpha_c = 0$, also the in-

Table 1. Galaxy mass and wind evolution

Model	r_h (kpc)	$M_*(t_G)$ (10^{11} M$_\odot$)	$M_g(t_G)$ (M$_\odot$)	t_w (Gyr)	$t_{w,e}$ (Gyr)	$M_*(t_w)$ (10^{11} M$_\odot$)	$M_g(t_w)$ (10^{11} M$_\odot$)	M_w (10^{11} M$_\odot$)	$M_{w,Fe}$ (10^8 M$_\odot$)
1	2.5	1.32	1.70×10^7	1.09	1.49	1.39	0.58	0.72	2.74
2	3.5	2.38	4.73×10^7	1.17	1.60	2.53	1.28	1.42	4.93
5	5	5.90	2.76×10^8	1.25	1.99	6.05	3.36	4.22	12.7
10	7	11.6	2.06×10^9	1.51	2.68	11.5	6.73	6.45	25.1
20	10	23.7	2.77×10^{10}	1.65	3.56	22.0	14.0	12.0	31.6
50	15	66.4	2.14×10^{11}	2.22	5.40	59.3	34.0	18.2	49.8
2(1/3)	3.5	2.83	5.23×10^7	1.32	1.69	3.03	0.94	1.10	5.60
2(0)	3.5	1.33	1.49×10^7	0.044	0.373	0.65	1.34	0.68	3.96

termediate mass stars produces only secondary N, so [N/H] has a smooth evolution all the way until several times 10^8 yr, when it reaches highly supersolar values. However, in the case $\alpha_c = 1.5$, [N/H] shows a steep rise at $\sim 3 \times 10^7$ yr due to the first primary N ejected by intermediate mass stars. Also note the fast increase of the abundances of α-elements (O, Mg), ejected by Type II SNe, which reach solar abundances at $\sim 10^8$ yr. By contrast, the enrichment of Fe is delayed with respect to that of O ([Fe/H] becomes solar at $\sim 3 \times 10^8$ yr) since Fe is mostly produced in Type Ia SNe, with long-lived progenitors.

3 EVOLUTION OF THE ISM AND STAR FORMATION RATE

We have built a sequence of galaxy models parameterized according to the total (initial) luminous mass inside the tidal radius, $M_G = M_g + M_*$ (the luminous mass of the galaxy is comprised by the stellar and the gas components, which are readly observable, mainly in optical and X-ray bands, respectively). The models are further characterized by r_h, r_t, and the ratio of the halo to the (initial) luminous mass, M_h/M_G. We have investigated a grid of runs with M_G between 10^{11} and 5×10^{12} M$_\odot$, and r_h in the range $2.5 - 15$ kpc. We set $r_t = 28 r_h$ and $M_h/M_G = 3$. The choice of the $r_h - r_t - M_G$ relation is based on the scaling laws of Sarazin & White (1987). ρ_{*0} and r_c of the stellar distribution are related to the central stellar velocity dispersion σ_* by the virial condition $4\pi G \rho_{*0} r_c = 9\sigma_*^2$. In addition, the model galaxies follow a Faber-Jackson relation, $\sigma_* = 200(L_B/L_B^*)^{1/4}$ km s^{-1} (Terlevich 1992), with L_B related to M_G through $[M/L_B] = 10$, the mass-light ratio typical of an L^* galaxy. In this work, we have chosen as fiducial model that one with $M_G = 2 \times 10^{11}$ M$_\odot$ and standard SFR. Due to inflow and galactic wind episodes occuring during the galaxy evolution, its present stellar mass is ~ 20% higher than the initial M_G. The fiducial model has $L_B = 2.4 \times 10^{10}$ L$_\odot$, i.e., somewhat fainter than the break luminosity of the Schechter luminosity function ($L_B^* = 3.7 \times 10^{10}$ L$_\odot$), and, therefore, is representative of the population of elliptical galaxies. In this work, since we are particularly interested in the relation between young galaxies and QSOs, we will explore a mass range corresponding to luminosities around and above L^*.

Table 1 summarizes the evolution of the gas and stellar components of the galaxy. The first column identifies the model: the number is M_G, the initial mass of the protogalaxy in units of 10^{11} M$_\odot$; the number between parenthesis is n_{SF} for models with $n_{SF} \neq 1/2$. In this paper we will identify the models by the codes in the first column of Table 1 (e.g. model 2 is the fiducial model). Column (2) gives r_h. Columns (3) and (4) show the present-day (at $t_G = 13$ Gyr) stellar and gas masses of the galaxy. The following columns exhibit characteristics of the galactic wind which appears in all models: t_w, the time of the onset of the galactic wind; $t_{w,e}$, the end of the early wind phase, defined by the gas mass being reduced to 10% of its amount at t_w; $M_*(t_w)$ and $M_g(t_w)$, the stellar and gas galaxy masses at t_w; M_w and $M_{w,Fe}$, the total and the iron masses ejected by the wind until t_G.

In this section, we investigate the evolution of the ISM and the star formation in our models. We now proceed to follow in some detail the evolution of the fiducial model. Since the initial conditions are out of equilibrium (the gas is initially cold), at the start of the calculations the gas falls towards the centre and is compressed, giving rise to shocks that rapidly heat the gas in the core to approximately the virial temperature of the system ($T \sim 10^7$ K). Then, a highly efficient star formation is occurring throughout the galaxy and a young stellar population is rapidly built up.

Following the initial violent star formation burst, the first Type II SNe appear at 3.2×10^6 yr, and shortly after, the SN heating dominates the energetics of the ISM. Fig. 2 shows the evolution of the supernova rates over the whole galaxy, normalized to the initial protogalactic mass (2×10^{11} M$_\odot$), for the fiducial model. The SN II rate reaches a maximum of 155 SNe (100 yr)$^{-1}$ (10^{11} M$_\odot$)$^{-1}$ at 3.9×10^8 yr and decreases rapidly after 1 Gyr. The broad maximum of the SN II rate reflects the ongoing star formation during the first Gyr of the galaxy. The present SN II rate is negligible (3.8×10^{-4} SNe (100 yr)$^{-1}$ (10^{11} M$_\odot$)$^{-1}$ at 13 Gyr). The Type II SNe are followed by the Type I SNe, which appear at 2.9×10^7 yr and attain a maximum rate of 19 SNe (100 yr)$^{-1}$ (10^{11} M$_\odot$)$^{-1}$ at 7.6×10^8 yr. After 1 Gyr, the SN I rate decreases less rapidly than the SN II rate and its value at $t_G = 13$ Gyr is 0.20 SNe (100 yr)$^{-1}$ (10^{11} M$_\odot$)$^{-1}$. Given $M_*(t_G) = 2.38 \times 10^{11}$ M$_\odot$ and $[M/L_B] = 10$, this value corresponds to 0.17 SNU (1 SNU = 1 SN (100 yr)$^{-1}$ (10^{10} L$_{\odot B}$)$^{-1}$) and is bracketed by observational estimates of the SN I rate: 0.22 h_{50}^2 SNU (Tammann 1982), 0.25 h_{50}^2 SNU (van den Bergh & Tammann 1991), 0.03-0.09 h_{50}^2 SNU (Capellaro et al. 1993), and 0.06-0.11 h_{50}^2 SNU (van den Bergh & McClure 1994). Only the SN I rate is significant in the later evolutionary phases ($t > 2$ Gyr) of the elliptical, when the star formation rate plummets and the SN II rate is drastically reduced. The late evolution of the SN I rate in the fiducial model can be approximated by a power law ($\propto t^{-1.77}$ from 1 to 13 Gyr). However, the power law be-

Figure 2. The evolution of the supernova rates for the fiducial model. The rates have been normalized to the initial protogalactic mass (2×10^{11} M$_\odot$).

Figure 3. The velocity profile of the gas for the fiducial model at several evolutionary times. The lines are labelled according to the time (in Gyr) they represent. The top panel allows one to follow the global inflow stage of the evolution of the ISM and the lower panel shows the partial wind ($t = 1.2$ and 1.6 Gyr) and the total wind stages ($t = 2$, 5, and 13 Gyr).

haviour cannot be extrapolated to the first Gyr of the model galaxy, since the plateau of the SN I rate between 0.5 and 1 Gyr is not reproduced.

The evolution of the gas velocity profile is shown in Fig. 3. Three stages can be distinguished in the evolution of the galaxy ISM. The first stage is a *global inflow* extending from the model inner boundary to the tidal radius. At the beginning of this stage, the inflow rises from the settling of the gas into the potential well of the dark halo. When the central density has increased enough to allow radiative losses to be important, a vigorous cooling flow is established in the inner kpc. Later during this stage, after the first SNe appear, the SN heating drives a wind at intermediate radii, separating the global inflow into an inner cooling flow feeding the galaxy nucleus and an outer inflow falling towards the galaxy. The wind advances towards the tidal radius and when it reaches the tidal radius at $t_w = 1.17$ Gyr, the second stage begins, characterized by a *partial wind*, i.e., a cooling flow in the inner regions of the galaxy and a wind in the outer regions. t_w is to be identified with the onset of the galactic wind. As more gas is consumed by star formation and expelled by the wind, the stagnation region separating the inner cooling flow from the wind moves inwards, and at 1.8 Gyr the cooling flow has shrunk into the inner boundary, so that a wind is established from 100 pc to the tidal radius, characterizing the third, *total wind* stage. The wind at the tidal radius reaches a peak velocity of 1860 km s^{-1} at 2 Gyr, and decreases afterwards, as the SN heating reduces due to the SN I rate decrease.

Fig. 4 shows the evolution of the stellar mass and gas fraction for the fiducial galaxy. From the mass evolution results of Table 1 and Fig. 4, it is clear that the gas is a major component of the galaxy during the first Gyr of evolution. Gas is turned into stars by a high star formation rate, but the gas consumption is not complete, since the continuous gas infall constantly supply the galaxy with gas. For the fiducial model, the SFR is initially higher than the infall rate leading to a decrease of the gas fraction as the stellar body of the galaxy is built up. The maximum SFR is ~ 500 M$_\odot$ yr^{-1} at 6×10^8 yr. By then the stellar mass is 2×10^{11} M$_\odot$. When the SFR has decreased to ~ 200 M$_\odot$ yr^{-1} at 8×10^8 yr, the infall rate overtakes the SFR, and the gas fraction reaches a minimum of 0.3 and then starts to increase again. The increase of the galaxy mass due to infall goes on until the onset of the galactic wind, at $t_w = 1.17$ Gyr. At this time, the galaxy mass has almost doubled ($M_G(t_w) = 3.8 \times 10^{11}$ M$_\odot$), and approximately one third of the galaxy mass is in the form of gas. The galactic wind that follows is so massive that almost all the remaining gas is removed from the galaxy. The gas expelled with the galactic wind represents a significant fraction of the galaxy mass (1.3×10^{11} M$_\odot$ from t_w until 13 Gyr). The gas removal is very fast: 50%(90%) of the gas is expelled in 2.3×10^8 yr (4.3×10^8 yr) after t_w. In later stages of evolution, stellar losses continue to supply mass to the wind, which in turn depletes the gas. During this epoch, the level of star formation is very low, and, as a consequence, newly formed stars do not replenish the dying stars, and the stellar mass decreases by 6 % from t_w until now. The net result of the early inflow, galactic wind and stellar losses is that the present-day galaxy mass is ~ 20 % higher than the initial protogalactic mass. For other galaxy masses, there is also an increase of mass, in the range of $15 - 30$%, but with no clear trend of $M_*(t_G)/M_G$ with M_G. The model with $n_{SF} = 1/3$ has a somewhat larger increase of 42%. The only discrepancy is represented by model 2(0), anomalous in many ways, in which the galactic wind occurs very early and leads to a reduction in mass of 34%.

Figure 4. Evolution of the stellar mass (solid line) and of the gas fraction (dotted line) for the fiducial model.

In this model, due to the weak dependency of the SFR on the density, the SFR is proceeding at high efficiency in the outskirts of the galaxy and the resulting SN heating avoids the massive initial infall typical of the other models.

Fig. 5 (top panel) shows for the fiducial model the evolution of the total SFR (over the whole galaxy) and of the inner SFR (inside the inner kpc). The total SFR initially has a value of 230 $\mathrm{M}_\odot\ \mathrm{yr}^{-1}$. As more fresh gas of the early inflow falls into the galaxy, the gas is compressed thus reducing the star formation time scale. Accordingly, the SFR rises up to a maximum of 480 $\mathrm{M}_\odot\ \mathrm{yr}^{-1}$ at 6×10^8 yr. During the first Gyr, the SFR is typically around 300 $\mathrm{M}_\odot\ \mathrm{yr}^{-1}$. At ~ 1 Gyr, the depletion of gas by star formation, reduces the SFR below 100 $\mathrm{M}_\odot\ \mathrm{yr}^{-1}$. The onset of the galactic wind at 1.17 Gyr leads to a drastic reduction of the SFR to $\sim 10^{-2}$ $\mathrm{M}_\odot$ yr^{-1} in less than 0.5 Gyr. While the total SFR shows more or less constant levels during the first Gyr of evolution, the inner SFR (inside a radius of 1 kpc) shows dramatic variations, due the short time scales for replenishment of gas and inhibition of star formation. It varies from 0.9 $\mathrm{M}_\odot\ \mathrm{yr}^{-1}$ at $t = 0$ to a maximum of 70 $\mathrm{M}_\odot\ \mathrm{yr}^{-1}$ at 7×10^8 yr, with several brief starburst episodes. Over the first Gyr of evolution, the inner SFR shows a typical range of $20 - 50$ $\mathrm{M}_\odot\ \mathrm{yr}^{-1}$. Note that, from the observational point of view, the inner SFR is more interesting than the total SFR, because only the inner regions of the galaxy, due to their higher surface brightness, would have star formation activity detectable at high redshifts.

We have calculated for the fiducial model the evolution of the bolometric luminosity of the stellar population of the whole galaxy (top panel of Fig. 5) by using the models of spectrophotometric evolution of Bruzual & Charlot (1993). Initially, the luminosity increases steadly while a young stellar population is being built up. At 3.3×10^8 yr, the young stellar population reaches 10^{11} $\mathrm{M}_\odot$. A maximum luminosity of 2.3×10^{12} $\mathrm{L}_\odot$ is reached at 6.1×10^8 yr, when the stellar mass is 2×10^{11} $\mathrm{M}_\odot$. The peak in luminosity closely follows the maximum in SFR, since at this time the main contribution to the luminosity comes from high-mass stars. It should be noted that the luminosities of our models are more than one magnitude lower than the luminosities in HF93. The HF93 model M4, intended to represent a giant elliptical, has a peak bolometric luminosity of 2×10^{13} $\mathrm{L}_\odot$ at 0.1 Gyr for a galaxy mass of 10^{11} $\mathrm{M}_\odot$, corresponding to a luminosity of 4×10^{13} $\mathrm{L}_\odot$ for the mass of the fiducial model. Part of this discrepancy arises from the flatter IMF ($x = 1.1$) assumed by HF93 in model M4, but most of it comes from the fact that HF93 models consider that the whole galaxy is involved in a starburst. In model M4, the SFR reaches a pronounced maximum very rapidly at 0.1 Gyr and then falls very rapidly. The time scale for star formation over the whole galaxy is $\sim 10^8$ yr. In our models, by contrast, the SFR keeps approximately the same levels during the first Gyr of the galaxy.

Figure 5. Top panel: evolution of the SFR over the whole galaxy and over the inner kpc (upper and lower solid lines, respectively), and the evolution of the bolometric luminosity of the stellar population of the whole galaxy in the fiducial model (dotted line). Lower panel: evolution of the specific SFR averaged over the inner kpc (upper line) and over the whole galaxy (lower line).

The lower panel of Fig. 5 shows the evolution of the average specific SFR inside the inner kpc and over the whole galaxy. The star formation time scales in the inner region are much shorter than over the whole galaxy. At the beginning of the calculations the star formation time scale is 1 Gyr over the whole galaxy and 10^8 yr in the inner kpc. The average specific SFR over the whole galaxy is typically between 1 and 3 Gyr^{-1} during the first Gyr. Note that only the central region of the galaxy is undergoing a violent starburst. The average specific SFR inside 1 kpc is typically ~ 30 Gyr^{-1} during the first Gyr. The one-zone models of HF93 overestimate the luminosity of the galaxy, because they assume over the whole galaxy a very short time scale of star formation ($\sim 10^8$ yr) in order to reproduce the fast metal enrichment needed to account for the metal lines observed in high redshift QSOs and the high [Mg/Fe] ratio in the nuclei of ellipticals. But these constraints need to hold only in the core of the galaxy. In a multi-zone model, only the inner region of the galaxy shows these very short time scales for star formation, while a relatively modest star formation efficiency characterizes the whole galaxy, leading to much lower luminosities than in the one-zone models.

4 THE GALACTIC WIND

In the early stages of the evolution of the galaxy, the gas content is always high. Gas is turned into stars by a high star formation rate, but the gas consumption is never complete, because the global infall constantly supply the galaxy with gas. The increase of mass due to infall goes on until the onset of the galactic wind. The wind then removes almost all gas from the galaxy. As in the classic SN-driven wind models, the onset of galactic wind occurs later for the more massive galaxies(see Table 1). In addition, the wind removes gas slower in more massive galaxies: the duration of the early wind phase increases steadly from 0.40 to 5.4 Gyr, as M_G varies from 10^{11} M$_\odot$ to 5×10^{12} M$_\odot$. For all models, the wind occurs later than 1 Gyr. The only exception is again model 2(0), for which the galactic wind occurs very early at 4.4×10^7 yr. For most of the models, the galactic wind persists until the present. However, in the most massive models 20 and 50, the very deep potential well causes the wind to be reversed to outer inflow at 11.8 and 8.8 Gyr, respectively, so these models do not exhibit galactic winds at the present epoch. Note that in a cluster environment, the higher pressures and densities at the outer boundary could cause outer inflows even in less massive galaxies.

As shown in Fig. 6, the galactic wind can be very metal-rich. The central gas abundances soon become supersolar: at $r = 100$ pc, [O/H]>1 at $\sim 10^8$ yr, and [Fe/H]>1 at $\sim 3\times10^8$ yr. After the wind has developed in the intermediate region of the galaxy, a metal-rich gas front advances outwards. At the onset of the galactic wind ($t_w = 1.17$ Gyr), the gas metallicity at r_t is low ([O/H]=1.2×10^{-2} and [Fe/H]=1.1×10^{-2}), although in the inner regions the gas is metal-rich ([O/H]=2.9 and [Fe/H]=5.6 at 1 kpc). There is a delay between mass removal and metal removal by the wind. When 90% of the gas has been removed (at 1.59 Gyr), the metallicity at the tidal radius ([O/H]=0.8 and [Fe/H]=1.4) is still low in comparison to the inner abundances ([O/H]=3.2 and [Fe/H]=8.9 at 1 kpc). Only at 1.77 Gyr, the metal-rich gas front reaches the tidal radius ([O/H]=1.3 and [Fe/H]=8.1 at r_t), and a shallow gas abundance gradient is established. After this time, the galactic wind is very metal-rich. The maximum metallicity is reached at ~ 2 Gyr, ([O/H]=1.3 and [Fe/H]=8.9 at r_t) and then decreases due to the dilution effect of stellar mass loss, as a higher fraction of H-rich gas is restored by lower-mass stars. The present-day metallicity of the gas is still high ([O/H]=1.1 and [Fe/H]=3.0 at r_t). It is interesting to note that the oxygen gradient is steeper than the iron gradient ([O/H]=2.8 and [Fe/H]=3.9 at 1 kpc).

Since the gas removed with the wind represents a mass amount comparable to the stellar component of the galaxy, it will have an important impact on the intracluster or intragroup medium where the galaxy is located. In particular, the galactic wind carries metals synthesized by the stars and therefore it is of great importance for the understanding of the chemical enrichment of the intergalactic medium. The results of our models confirm the suggestion that elliptical galaxies could explain the iron abundances in the intracluster medium (ICM) of X-ray clusters of galaxies (David et al. 1990,1991). It is interesting to note that the late wind phase (i.e. from $t = 1.60$ Gyr on) makes the more important contribution to the iron enrichment. Only 6.9×10^7 M$_\odot$ of iron is expelled during the early wind phase, that is, 14% of all iron ejected by the galaxy. The oxygen enrichment of the intracluster medium occurs much earlier, with 4.7×10^8 M$_\odot$ being expelled during the early wind phase, i.e. half the total amount of oxygen (9.83×10^8 M$_\odot$) ejected by the present epoch. This result is not unexpected, since iron arises mostly from Type Ia SNe and the longer lifetimes of the Type Ia SN progenitors result in a delayed Fe enrichment. By contrast, the early wind removes gas pre-enriched by α-elements produced in Type II SNe during the first few 10^8 yr of evolution. In any case, one should take note of the important delays in the enrichment of the ICM represented by the time scale $t_{w,e}$, which is $\gtrsim 1.5$ Gyr for galaxies brighter than $\sim 0.1L^*$, and in the case of iron enrichment, by the arrival time of the Fe-rich front at the boundary of the galaxy (1.77 Gyr for the fiducial model).

Figure 6. [Fe/H] and [O/H] radial profiles of the gas for the fiducial model at several epochs: 0.03 Gyr (solid line), 0.35 Gyr (short-dashed), 1 Gyr (long-dashed), 1.6 Gyr (dotted), 1.9 Gyr (dot-short-dashed), 4.4 Gyr (dot-long-dashed), 13 Gyr (short-dashed-long-dashed).

The iron contribution to the ICM by the ellipticals could be checked through the quantity $(M_{Fe}/L_B)_{cl}$, introduced by Ciotti et al. (1991) (here, M_{Fe} is the total iron mass in the ICM and L_B is the integrated blue luminosity of the galaxies of the cluster). Elliptical galaxies contribute most of the luminous mass in the most X-ray luminous clusters. In the fiducial model, the galactic wind ejects until the present

Table 2. Present-day stellar chemical abundances

Model	$\langle[Mg/H]\rangle_1$	$\langle[Fe/H]\rangle_1$	$\langle[Mg/H]\rangle_{10}$	$\langle[Fe/H]\rangle_{10}$
1	2.20	1.38	1.30	0.716
2	2.57	1.53	1.38	0.754
5	2.59	2.05	1.54	0.943
10	3.40	2.22	1.58	0.935
20	3.52	2.89	1.58	0.979
50	4.30	3.98	1.69	1.420
2(1/3)	2.59	1.65	1.46	0.824
2(0)	1.57	0.66	0.77	0.283

4.93×10^8 M$_\odot$ of iron, which is mixed to the ICM. Considering this model as representative of the cluster ellipticals, and assuming $[M/L_B] = 10$ for the stellar mass in the cluster, from $M_* = 2.38 \times 10^{11}$ M$_\odot$ we obtain $(M_{Fe}/L_B)_{cl} = 2.1 \times 10^{-2}$ M$_\odot$/ L$_\odot$ in good agreement with the value inferred from observations, $(M_{Fe}/L_B)_{cl} \approx 10^{-2}$ M$_\odot$/ L$_\odot$ (Ciotti et al. 1991), therefore giving support to the thesis that enrichment by ellipticals explains the ICM iron abundances. The ratio $M_{w,Fe}/M_*$ is approximately constant $\approx 2 \times 10^{-3}$ over the mass range $M_G = 10^{11} - 10^{12}$ M$_\odot$ and also for the model 2(1/3). In the most massive models 20 and 50, this ratio is reduced to 1.4×10^{-3} and 7.5×10^{-4}, respectively, because the increase of the iron abundance as a result of a longer building-up time does not counterbalance the decrease of the fraction of mass ejected with the depth of the potential well. In model 2(0), the higher $M_{w,Fe}/M_*$ (3×10^{-3}) is due to the large amount of metals ejected with the wind, with little metal being locked in stars.

We should take note of one possible problem regarding the iron abundances of the wind predicted by our models, which are too high in comparison to those derived from X-ray observations. From BBXRT observations and one-temperatures fits, Serlemitsos et al (1993) have estimated the metallicity of NGC 1399 and NGC 4472 to be 0.18-1.38, and 0.11-0.66 times solar (90% confidence), respectively. This low abundance is in contradiction with *ROSAT* measurements of Forman et al (1994), who determined the iron abundance of NGC 4472 to be 1-2 times solar. A more extended sample of early-type galaxies observed with the ASCA satellite, however, has confirmed the subsolar abundances found by the BBXRT. The analysis of galaxies in the Virgo cluster, including NGC 4742, finds that the abundances of Fe and other elements are ~ 0.5 solar (Awaki et al. 1994; Matsushita et al. 1994); and exceptionally low abundances, $Z \sim 0.15$ solar, are derived for NGC 1404 and NGC 4374 (M84) located in the Fornax and Virgo clusters, respectively (Loewenstein et al. 1994). However, the present X-ray spectral analysis has several uncertainties that may lead to spurious results for abundances. For instance, problems have been encountered with the basic plasma emission models for the Fe L complex during the analysis of the ASCA spectra of the cooling flows in the Perseus, Centaurus and A1795 clusters (Fabian et al. 1994). The consistency of the spectroscopic data with the plasma emission models was achieved only with a recalculation of the Fe L-shell spectra with a novel atomic physics package and an update of the Fe data (Liedahl et al. 1995).

These low abundances, if real, severely constrain the Type Ia supernova enrichment of the ISM of early-type galaxies. In particular, the present SN Ia rate may be lower than that of our models. In fact, the SN I rate predicted by the fiducial model is at the upper end of the values derived from the observations; a reduction by 1/4-1/3 is still consistent with the observations. On the other hand, Type II SNe may have a larger share in the Fe enrichment of the ICM, either by an IMF flatter than the Salpeter one as the $x = 0.95$ IMF invoked by Arimoto & Yoshii (1987) to reproduce the broad-band colors of giant ellipticals, or by an increased lower-mass cutoff of the IMF, as in the high-mass mode of star formation, proposed for the early evolution of ellipticals (Elbaz, Arnaud, & Vangioni-Flam 1995). Another possibility is that the abundances in the hot gas arise from incomplete mixing of the supernova ejecta as relatively metal rich inhomogeneities cool very fast decoupling from the hot gas (Loewenstein et al. 1994). Finally, in the case of galaxies in clusters, the infall of gas from the ICM leads to metallicities in the X-ray galactic corona reflecting the subsolar abundances of the ICM.

5 ABUNDANCES OF THE STELLAR POPULATION

Table 2 shows the abundances of the stellar population at the present: $\langle[Mg/H]\rangle_1$ and $\langle[Fe/H]\rangle_1$, the Mg and Fe abundances mass-averaged over the inner kpc; $\langle[Mg/H]\rangle_{10}$ and $\langle[Fe/H]\rangle_{10}$, the Mg and Fe abundances mass-averaged inside 10 kpc (10 kpc is roughly the effective radius of an L^* galaxy). The code for the models is the same as in Table 1. The core ($r \lesssim 1$ kpc) of our model galaxies is metal-rich, in agreement with the metallicities of 2-3 for the nucleus of elliptical galaxies, derived from observations of the Mg$_2$ indices. For the fiducial model, both magnesium and iron exhibit central overabundances at the present ([Mg/H]=3.4 and [Fe/H]=2.5 at 100 pc; [Mg/H]=2.0 and [Fe/H]=1.2 at 1 kpc). At larger radii, however, the abundances become subsolar ([Mg/H]=0.67 and [Fe/H]=0.29 at 10 kpc), indicating the presence of abundance gradients in the galaxy stellar population.

Metallicity gradients for the stellar population of early-type galaxies have been inferred from measurements of line-strength gradients (Gorgas, Efstathiou & Salamanca 1990; Worthey, Faber & Gonzáles 1992; Davies, Sadler & Peletier 1993 Carollo, Danziger & Buson 1993; Fisher, Franx & Illigworth 1995). Fig. 7 shows the evolution of the magnesium and iron abundances of the stellar population at several radii for the fiducial model, allowing us to derive metallicity gradients. For $r > 1$ kpc, the abundance gradients predicted by

Figure 7. The evolution of [Mg/H] (solid curves) and [Fe/H] (dotted curves) of the stellar population at several radii for the fiducial model. The upper, the middle and the lower curves refer to radii of 100 pc, 1 kpc, and 10 kpc, respectively. Note that the $r = 100$ pc and $r = 1$ kpc curves, for both [Mg/H] and [Fe/H], *do not* cross.

our models are higher than the average logarithmic abundance gradient ($d \log[\mathrm{Fe/H}]/d \log r$) of -0.2 derived by Davies et al. (1993) from line-strength gradients measured out to distances of 5-20 kpc from the centre of the galaxy. For the magnesium, the present abundance gradients of the fiducial model are -0.22 for 100 pc $< r <$ 1 kpc and -0.48 for $1 < r <$ 10 kpc, and for the iron, the respective values are -0.32 and -0.60. The abundance gradients are expected to be flatter when the dependence of the SFR on density is weaker. This is confirmed by the model 2(1/3) which exhibits magnesium (iron) abundance gradients of -0.18 (-0.28) for 100 pc $< r <$ 1 kpc and -0.49 (-0.61) for $1 < r < 10$ kpc, although the abundance gradients do not change dramatically. It should be noted that our models tend to overestimate the abundance gradients, since the stars are moved only to reproduce a King profile: the newly formed stars are stored in shells, and each shell is moved as a whole entity to their final position. Our models do not include orbital mixing, i.e., the distribution of orbits of individual stars, in which case the stars at a given radius would have apocentres spanning a wide range of radii. The inclusion of orbital mixing would lead to the flattening of the metallicity gradients. This effect, however, would have little impact on the central abundances of the galaxies.

Note that a high metallicity stellar core is rapidly built up. The central stellar magnesium abundance becomes supersolar at 1.9×10^8 yr and the iron abundance at 8.3×10^8 yr, respectively. Therefore, the conditions required by the starburst model of QSOs (TB93), a metal-rich stellar population and a metal-rich ambient gas (as seen in Section 4), are achieved in the early stages of the evolution of ellipticals.

One important constraint to chemical evolution is given by abundance ratios derived from Mg and Fe line strengths (based on Mg_2, Fe5270 and Fe5335 indices). It seems that Mg is overabundant with respect to Fe in giant ellipticals. The ratio [Mg/Fe] exhibits a large scatter around 1.5-2.0 (Worthey et al. 1992). This high ratio is interpreted as a signature of enrichment by Type II SNe, implying that the formation of an elliptical was very rapid, otherwise the iron enrichment by Type Ia SNe would have shifted the [Mg/Fe] ratio to solar or subsolar values. Our models predict a range of $1.1 - 1.8$ for [Mg/Fe]. This reproduces well the observations, indicating that the star formation time scale of 10^8 yr chosen as normalization of the SFR based on results of one-zone models, is also appropriate for the our dynamical model. Again, model 2(0) is discrepant from the rest. As a consequence of the very early galactic wind [Mg/Fe] is shifted to very high values, $2.4 - 2.7$, due to a very high dominance of SN II in the chemical enrichment, and little metal is locked in the stars, so the core is not metal-rich.

One important result we can derive from Table 2 is that the metallicity increases with the galaxy mass, and thus the well-known metallicity-mass relation for ellipticals is reproduced by our models. The trend of increasing metallicity with mass is stronger for the abundances averaged inside a smaller aperture. For a larger aperture, the metallicity-mass relation is less smooth. The metallicity-mass relation is a consequence of the occurrence of galactic winds, which appear later for galaxies with deeper gravitational wells, thus allowing more metal enrichment for the gas and the stars formed from it, a mechanism first suggested by Larson (1974b). The consistency of the galactic wind scenario can be seen from the results of Table 1, which shows that, given a star formation law, the time for the onset of the galactic wind increases with the galaxy mass.

One further prediction from Table 2 is a clear, although not strictly monotonic, trend of decreasing [Mg/Fe] ratio with the galactic mass: for the models with standard SFR, $\langle[\mathrm{Mg/Fe}]\rangle_1$ ($\langle[\mathrm{Mg/Fe}]\rangle_{10}$) shows a maximum of 1.68 (1.83) for model 2 (note that the respective values for model 1 are 1.59 and 1.82) and a minimum of 1.08 (1.19) for model 50. However, this prediction seems to be at variance with the observations of the stellar population in ellipticals, which suggest a slight trend of increasing [Mg/Fe] ratio with the galactic luminosity, albeit with a large scatter (Worthey et al. 1992, Weiss, Peletier & Matteucci 1995). The reason for the increase of [Mg/Fe] with M_G in our models is that, under the our assumption of star formation time scale independent of galactic mass ($\nu_0^{-1} = 10^8$ yr), the galactic wind happens later for more massive objects. As a result, the [Mg/Fe] ratio tends to decrease with the galactic mass because the bulk of iron is produced by type Ia SNe with a ~ 1 Gyr delay relative to the α-elements, produced by type II SNe on much shorter time scales. Note that, for the sake of simplicity, our models assume that: 1) the specific SFR is independent of the galactic mass; 2) the IMF is the same for all elliptical galaxies (see Matteucci 1994). If we relax the assumption 1), the predicted [Mg/Fe] trend could be conciliated with the observations if the star formation in giants ellipticals is faster than in smaller ellipticals, so favouring magnesium production over iron production. Another way to achieve a increase of [Mg/Fe] with the galactic mass is a variable IMF, with the slope of the IMF decreasing with the galactic mass, which leads to a larger proportion of massive stars in larger galaxies, and, as a consequence, to a larger α-element enhancement in more massive galaxies.

6 EVOLUTION OF THE LUMINOSITY OF QSOS

The luminosity function (LF) of QSOs undergoes strong evolution between $z = 2$ and the present epoch, with the redshift dependence of the LF being well-described by a constant comoving space density and a pure power-law luminosity evolution $L(z) \propto (1+z)^k$ (Boyle et al. 1988, 1991, BT98). Estimates of the rate of evolution k lie in the range $3.1 < k < 3.6$, corresponding to an evolution in terms of cosmic time t of the form $L_{QSO}(t) \propto t^{-n}$, with $2 < n < 3.5$, depending on the choice of cosmology.

Both in the supermassive black hole scenario and in the starburst model for AGN, the QSO luminosity evolution is linked to the mass flow into the galactic nucleus. In both cases the QSO luminosity is proportional to the average mass accretion rate, via either gravitational energy (supermassive black hole) or massive stars activity (starburst model). Two central assumptions are common to both approaches to explain the luminosity function of QSOs: 1) the luminosity of the QSO is proportional to the mass of the host galaxy; and 2) virtually all bright galaxies have harboured a QSO (AGN) during their evolution.

Our models develop a central cooling flow as soon as the gas central density has increased enough to allow radiative losses to be important. The cooling flow extends over a considerable span of their evolution, and, in most cases, when enough gas has been consumed by star formation or removed by gas flows, SN heating becomes more important than radiative cooling, and the central cooling flow is extinguished. As shown below, the fate of the central cooling flow depends on the galaxy mass and the star formation law. We now proceed to investigate whether the time-dependency of the central cooling flow rate in our models could be responsible for the observed evolution of QSOs.

Table 3 gives relevant information about the evolution of the central cooling flow for several models (see Table 1 for the keys to the models): $M_c(t_G)$, the mass deposited by the central (into the inner 100 pc) cooling flow until the present; N_{cf}, the number of cooling flow episodes until the present; $t_{cf,1}$ and $M_{c,1}$, the duration and the total mass deposited by the first cooling flow episode; M_c^*, the mass deposited by the cooling flow until $t = 1$ Gyr; $\zeta = M_{c,1}/M_G(t_G)$ (this parameter relates the present-day galaxy mass to the mass of galactic nucleus at high-redshifts). The end of the first central cooling flow episode is defined when the central cooling flow rate $\dot{M}_c = 0$ or, if the central cooling flow never vanishes, when $\dot{M}_c$ reaches a minimum.

Fig. 8 shows the evolution of $\dot{M}_c$. In order to compare to the observed LF evolution (Boyle et al. 1988, 1991, BT98), we fitted a power law to $\dot{M}_c$ between $t = 1$ Gyr and $t_{cf,1}$. The values of the index $n_{c,1}$ of the fit $\dot{M}_c \propto t^{n_{c,1}}$ are shown in Table 3. As we can see from M_c^* (Table 3), $\approx 70-80$ % of the total mass of the first central inflow have been deposited in the galactic nucleus by 1 Gyr. This time is the typical time scale for the completion of the large spheroids. If we consider that this event concides with the QSO phenomenon, the epoch when the QSO activity was at its peak ($2 < z < 3$) (Schmidt et al. 1991) corresponds to the epoch of galaxy formation $3.21 < z_{GF} < 6.54$ Gyr, a reasonable range in a number of scenarios for galaxy formation.

As seen in Section 3, the initial global inflow stage is followed by a partial wind stage, during which a wind is established in the outer regions of the galaxy. The stagnation region separating the wind and the inflow moves inwards until only a wind is present throughout the galaxy. In some cases, the total wind persists until the present epoch and no material restored by the stars is accumulated in the galaxy. That is the *single partial wind* sequence (the partial wind occurs only once),

global inflow → partial wind → total wind.

In some models, however, after some time, the gas in the inner regions is not swept out rapidly enough and starts accumulating until a central cooling flow is established again. The occurrence of the late partial wind characterizes a second type of gas flow sequence, the *multiple partial wind* sequence

global inflow → partial wind → total wind → partial wind...

The three models which exhibit late partial winds — models 10, 20, and 2(1/3) — illustrate the three possible fates of the late partial wind. In the first place, the partial wind could persist until the present (model 10). Other possibility is that it develops into a global cooling flow extending from the nucleus to the tidal radius of the galaxy. That is the case of model 20, in which the outer wind reverses to outer inflow at 11.8 Gyr. Finally, the central inflow could be halted by supernova heating due to the resulting starburst occurring in the galaxy core, as in model 2(1/3). There is one further type of gas flow sequence, in which the total wind never occurs, that is,

global inflow → partial wind → global inflow.

This sequence is exhibited by the very massive model 50. In this model, the central cooling flow is never turned off, and more than 10^{10} $M_\odot$ has been deposited into the nucleus by the present epoch. Due to the large potential well of the galaxy, the galactic wind stalls early and an outer inflow is established at 8.8 Gyr.

As seen from Fig. 8, in our models, the central inflow rate exhibits a large variety of evolutionary sequences, some of which combine features of the continuous and recurrent activity, exhibiting in many cases late cooling flow episodes, which can be weak or vigorous, short- or long-lived. All the models, however, show during the first Gyr a massive deposition rate, followed by a declining accretion rate evolution. The first central cooling flow episode, common to all models, extends for $2-3$ Gyr. The early evolution of the first cooling flow is subject to considerable fluctuations. An early, secondary maximum is apparent between 30 and 60 Myr, and it is followed by a decrement in the inflow rate, as the heating due to Type II SNe inhibits the cooling flow. From 10^8 yr on, the inflow rate increases until it reaches the absolute maximum. By then, and during the following decline of $\dot{M}_c$, the evolution is relatively smooth. The peak inflow rate occurs at $0.38-067$ Gyr for the models with $n_{SF} = 1/2$, and is earlier for the most massive models. For model 2(1/3), it is at 0.94 Gyr, and for model 2(0), it is at 0.17 Gyr.

Table 3. Central cooling flow properties

Model	$M_c(t_G)$ (10^8 M$_\odot$)	N_{cf}	$t_{cf,1}$ (Gyr)	$M_{c,1}$ (10^8 M$_\odot$)	M_c^* (10^8 M$_\odot$)	ζ (10^{-3})	$n_{c,1}$
1	5.20	1	1.80	5.20	4.15	3.94	-2.53
2	6.74	1	1.80	6.74	5.53	2.83	-3.58
5	13.2	1	2.23	13.2	9.72	2.24	-3.23
10	17.9	2	2.81	17.4	12.6	1.50	-4.25
20	51.7	2	2.78	35.2	24.3	1.52	-4.28
50	185	2	3.16	97.1	67.4	1.46	-3.68
2(1/3)	8.48	3	2.04	8.24	6.05	2.91	-3.02
2(0)	1.76	1	1.36	1.76	1.62	1.32	-2.16

The fit to the declining part of the evolution of the cooling flow rate by $\dot{M}_c \propto t^{n_{c,1}}$ gives values of $n_{c,1}$ in the range $-4.3 < n_{c,1} < -2.5$. The values of $n_{c,1}$ refers only to the first cooling flow episode and describe only the 1-3 Gyrs following the maximum in $\dot{M}_c$. The principal conclusion that $n_{c,1}$ (and $t_{cf,1}$) allows us to derive is that, under the assumption of proportionality of the luminosity to $\dot{M}_c$, the most active phase of the QSO is likely to occur during a short span of time since the galaxy formation and that the early evolution of luminosity is very steep, which is consistent with the derived evolution of the QSO LF.

One particularly interesting model is 2(1/3) because it exhibits recurrence of late central inflow episodes. As the SN I rate decreases, the wind stalls, the gas starts accumulating in the galaxy core, and the radiative losses drive a new central cooling flow. The late central inflow episodes are brief and quickly put out by the resulting burst of star formation. The duration of the late cooling flow episodes is a few times 10^7 yr, and, since the separation between them is typically a few Gyr, their duty cycle is $\sim 1/100$. The turning on and off of the central inflow could correspond to the "active" and "inactive" states of the core in both the supermassive black hole model of AGN and the starburst model of AGN. In addition, the length of the duty cycle of the central inflow increases with time and the amount of material deposited decreases, implying a steep decrease of the time-averaged luminosity of any central activity powered by the infalling material. For the model 2(1/3), the second central inflow occurs at $t = 4$ Gyr and involves 1.5×10^7 M$_\odot$, and the third one of 8.4×10^6 M$_\odot$ happens at $t = 9.5$ Gyr. Note that also in model 20, the late central inflow episode at $t \sim 5$ Gyr is inhibited by SN heating, following the starburst in the galactic core. However, the deep potential well of this model guarantees that at the end a massive central inflow prevails.

Episodic models of QSO activity have already been put forward to explain the observed evolution of the QSO LF both in the supermassive black hole scenario (Cavaliere & Padovani 1986) and in the starburst model (TB93). In the starburst model, the SFR in the galactic core actually responsible for the AGN activity is represented by a series of narrow ($\sim 10^7$ yr) peaks. In this model, between $z = 2$ and the present, the galaxy core undergoes between 3 and 5 successive bursts of QSO activity, with their amplitude being modulated by a power law with time of the form $SFR_{max} \propto t^{-2}$. This power law evolution is found in the elliptical galaxy models of Larson (1974a), which, however, refers to a continuous evolution of the SFR instead of an episodic one.

It is interesting that just changing the star formation law from $n_{SF} = 1/2$ in the fiducial model to $n_{SF} = 1/3$ gives rise to the appearance of short episodes of inflow, lasting $\sim 3 \times 10^7$ yr, similar to those appearing in the episodic scenario. As matter of fact, the time scale above refers to the final, more vigorous part of the inflow episode, when the central inflow rate suddenly becomes larger than $10^{-2} - 0.1$ M$_\odot$ yr^{-1}. The total duration of each episode is some 10^8 yr, characterized in its first phase by an inflow at a low rate (cf. the left wing in the second cooling flow event of model 2(1/3) in Fig. 8). Once the inflow rate becomes larger, the cooling flow is extinguished by the resulting star formation burst. The fact that evolution of the inflow rate with recurrent late cooling flow episodes appears naturally in model 2(1/3) gives support to the episodic scenario of QSO activity.

The models with a deep potential well (models 10, 20 and 50) have massive cooling flows that are well-developed at the present, in some cases having been initiated very recently (model 10). In models 20 and 50, the late cooling flow is particularly large, with 1.3×10^9 M$_\odot$ and 8.8×10^9 M$_\odot$, respectively, accumulated in the nucleus during the second central inflow episode. These massive late cooling flows are distinct from the short-lived events required by the episodic models of QSO activity, in that their duration is ~ 1 Gyr or more.

The very massive model 50 allows us to investigate the ability of our models to account for the luminosities of the brightest QSOs. The present stellar mass (6.6×10^{12} M$_\odot$) of this model is representative of the most luminous ($M_B \approx -24$) ellipticals in the nearby Universe (corresponding to a stellar mass of 6.2×10^{12} M$_\odot$ for $[M/L_B] = 10$). Model 50 has a peak central inflow rate of 20 M$_\odot$ yr^{-1} at 3.8×10^8 yr. The expected bolometric luminosity $L_{Bol} = f\dot{M}c^2 = 5.7 \times 10^{46} f(\dot{M}/\,\mathrm{M}_\odot\,\mathrm{yr}^{-1})$ erg s^{-1}, is 1.1×10^{47} erg s^{-1}, for an efficiency f of mass-energy conversion of 0.1. This bolometric luminosity is typical of very bright distant QSOs, but it fails to explain the bolometric luminosities of the brightest QSOs ($\approx 10^{48}$ erg s^{-1}). It should be noted, however, that the bright end of the QSO LF is contaminated by luminosity overestimates due to beaming and gravitational lensing. In addition, the luminosity estimated above assumes that the mass flow rate through the inner 100 pc radius is directly deposited into the central energy source of the QSO. It is expected that the evolution of the central inflow rate will modulate any central activity inside the galaxy nucleus, but the present calculations do not intend to describe in detail the region inside the 100 pc radius. As a matter of fact, the interaction gas flow-central engine may take place at a much smaller scale than the inner boundary. In particular, the bolometric luminosity given above refers to a continu-

Figure 8. Predicted evolution of the central inflow rate $\dot{M}_c$ (binned over 20 logarithmic time intervals per decade). The panels are labelled according to the model codes of Table 1. The dashed lines represent power-law fits to $\dot{M}_c$ between $t = 1$ Gyr and the end of the first cooling flow episode.

ous deposition of gas fueling the luminosity. The gas may as well accumulate in the core during a long period and then be consumed in a much shorter "turning-on" time, either falling into a supermassive black hole or triggering a violent starburst. One useful time scale to constrain the turning-on time is the crossing time though $r_{in} = 100$ pc, $t_{cross} = r_{in}/\sigma$. From the Faber-Jackson relation, $t_{cross} = 5 \times 10^5$ yr for an L^* galaxy, and 2.5×10^5 yr for a galaxy with $M_B = -24$. If the turning-on time is $10^6 - 10^7$ yr, and the accumulation time 1 Gyr, the duty cycle is 10^{-3}–10^{-2}, a range expected in several models for QSO activity. By the time of peak deposition rate in model 50, the mass in the nucleus is 2.8×10^9 $\mathrm{M}_\odot$. By $t = 1$ Gyr, it is 6.7×10^9 $\mathrm{M}_\odot$. A burst of activity involving such amount of mass at a conversion efficiency $f = 0.1$ with a time scale of a few 10^7 yr, could explain the bolometric luminosity of even the most luminous QSOs. As a matter of fact, the limit luminosity to be attained by any sort of central engine inside the galaxy nucleus is the Eddington luminosity $L_E = 4\pi G M m_H c/\sigma_T = 1.4 \times 10^{38}$ $(M/\mathrm{M}_\odot)$ erg s^{-1}. For model 50 at $t = 1$ Gyr, $M_c = 6.7 \times 10^9$ $\mathrm{M}_\odot$ implies $L_E = 9.4 \times 10^{47}$ erg s^{-1}, a value that, even disregarding beaming effects, could explain the highest luminosities of QSOs. In addition if we take into account the trend of $[M/L_B]$ to increase with galaxy mass (Terlevich 1992), then the most luminous galaxies have $[M/L_B] \approx 20$ implying a larger mass than that inferred from the blue luminosity using $[M/L_B] = 10$. In this case, scaling the luminosities to model 50, L_E exceeds 10^{48} erg s^{-1}.

The evolution of M_c in our models allows us to make predictions about the QSO LF. Specifically, we now proceed to calculate the QSO LF in the redshift range $2.0 < z < 2.9$ in order to compare our results with the observational blue QSO LF of Boyle et al. (1991). In view of the energetic dificulties with the continuous evolution of activity, we assume that the luminosity of the QSO is due to short episodes of nuclear activity resulting from the fast consumption of the gas accumulated in the nucleus by the central inflow. For illustrative purposes we consider only the first inflow episode and that two nuclear activity events occur during the first central inflow. Based on the results of Table 3, we consider that the duration of the first inflow is 2 Gyr. We assume the first activity event at 1 Gyr and the second one at 2 Gyr. From the ratio $M_c^*/M_{c,1}$, we assume that 75 % of $M_{c,1}$ is consumed by the first event and 25 % by the second one. For the estimate of the LF of galactic nuclei at high redshifts, we need to scale the present-day elliptical galaxy LF both in luminosity and in space density. The present-day elliptical galaxy LF we adopt is (Terlevich 1992; TB93)

$$\Phi(M_B) dM_B = \Phi^* 10^{0.4(M_B^* - M_B)\beta} \exp[-10^{0.4(M_B^* - M_B)}] \, , \quad (6)$$

where $\Phi^* = 3.6 \times 10^{-4} \, h_{50}^3$ Mpc^{-3}, $M_B^* = -21$, and $\beta = 0.23$. This form represents well the LF of moderately bright ellipticals, but underestimates the LF both at the bright and the faint ends. Accordingly, a power-law extension for $M_B \leq -22.5$, $\Phi(M_B) dM_B \propto (L_B/L_B^*)^{-3}$, is included to represent the cD galaxy data (Terlevich 1992). One the other hand, recent determinations of the faint-end of the LF indicate a turn-up of the LF for luminosities fainter than $M_B = -17.5$ (Smith, Driver, Phillipps 1997). Therefore, following Smith et al., we add a dwarf Schechter LF with parameters Φ^*(dwarfs)$= 1.5 \times \Phi^*$(giants), $M_B^* = -17.5$, and $\beta = -0.7$, to represent the dwarf spheroidals.

The scaling of the luminosity L_B^k of the k-th nuclear activity event to the present-day elliptical galaxy luminosity L_B is given by

$$\begin{aligned} L_B^k &= (f/BC)\xi_k (M_c c^2/t_{on}) \\ &= (f/BC)\xi_k (c^2/t_{on}) \times \zeta \times [M/L_B] \times L_B, \qquad (7) \end{aligned}$$

where $BC = L_{Bol}/L_B$ is the nucleus bolometric correction factor, f is the efficiency of mass-energy conversion, M_c is the mass deposited by the first central inflow episode, ξ_k is the fraction of M_c consumed in the k-th activity event, t_{on} is the time-scale for gas consumption, $\zeta = M_c/M_*$, the ratio of M_c to the present-day galaxy stellar mass M_*, and $[M/L_B]$, the present-day elliptical mass-to-light ratio. The adopted $\zeta - M_*$ relation is derived from Table 3: $\zeta = 3.28 \times 10^{-2} - 2.59 \times 10^{-3} \log(M_*)$ for $M_* < 1.2 \times 10^{12}$ $\mathrm{M}_\odot$, and $\zeta = 1.5 \times 10^{-3}$ for larger masses. The increase of $[M/L_B]$ with $|M_B|$ is represented by $[M/L_B] = -1.90 - 0.138 M_B$ (Terlevich 1992) for $-18.8 \geq M_B \geq -23.2$, with $[M/L_B] = 20$ for higher luminosities and $[M/L_B] = 5$ for lower luminosities.

In order to scale in density number we assume that the galaxies are formed uniformly in time during the epoch $3 < z_{GF} < 10$. Considering that the high-redshift QSO activity is signalled by the first nuclear activity event which occurs when the galaxy is 1 Gyr old, the correponding epoch of nuclear activity is $1.86 < z < 3.52$. This span in redshift is consistent is the strong decline of QSO counts for $z < 2$ and $z > 3.5$ (Boyle et al. 1991, Warren et al. 1994). The scaling in density is then obtained by multiplying the present-day elliptical galaxy LF by the duty cycle $\kappa = t_{on}/t_{off}$ ($t_{off} = t(z = 3) - t(z = 10) = 1.33$ Gyr).

Fig. 9 illustrate the predictions of our models for the $2 < z < 2.9$ LF of the galaxy nucleus, combining the two

Figure 9. Predicted galactic nuclear $2 < z < 2.9$ LF within both the massive black hole (dotted line) and the starburst (dashed line) scenarios. Also shown (dot-dashed line) the evolution of the LF predicted by a formal best fit model (see text). between $2.00 < z < 2.90$ and $1.25 < z < 2.00$. The LF data of Boyle et al. (1991) are also given for the same redshift intervals (symbols connected by solid lines).

activity events described above, for both the massive black hole and the starburst scenarios. The relation $L_B^k - L_B$ can be rewritten in a convenient way as

$$L_B^k/L_B = 14.7\,(f_{0.1}/BC_{10})\xi_k(\zeta_{-3}/t_{on,7})[M/L_B], \qquad (8)$$

where $f_{0.1} = f/0.1$, $BC_{10} = BC/10$, $\zeta_{-3} = \zeta/10^{-3}$, and $t_{on,7} = (t_{on}/10^7\ \mathrm{yr})$. In the calculation of t_{on}, we assume that $t_{on} \propto t_{cross}$ or $t_{on} = t_{on}^*(L_B/L_B^*)^{-1/4}$. In addition, t_{on} is constrained by the Eddington time $t_E = \sigma_T c/4\pi G m_H$ ($t_{on} \geq f\,t_E = 4 \times 10^7 f_{0.1}$ yr) and, in the starburst model, by the lifetime of the typical star giving the luminosity of the starburst ($t_{on} \geq t_m(\langle m \rangle)$). For the massive black hole model, we consider a rather conventional set of values $f_{0.1} = 1$, $BC_{10} = 1$, and $t_{on,7}^* = 3$. The values $f_{0.1} = 0.05$, $BC_{10} = 0.6$, and $t_{on,7}^* = 1$ are used in the starburst model. We consider that the starburst is dominated by very massive stars, e.g. $\langle m \rangle \approx 25$ M$_\odot$, since the standard star cluster of TB93 model would not be energetically feasible. From the fact that, for a 25 M$_\odot$ star, $\sim$ 17 M$_\odot$ have been converted into helium and carbon at the end of the C-burning phase with a convertion efficiency of 0.007, we obtain $f = (17/25) \times 0.007 = 0.005$. The value $BC = 6$, although low, has been previously considered in calculations of the QSO LF within both the massive black hole and the starburst scenarios (Haehnelt & Rees 1993, Terlevich 1994). The starburst considered in the present model differs from that in TB93 model in that here, we focus only on the galactic nucleus (with $0.15 - 0.5$ % of the galaxy mass and $r < 100$ pc). In contrast to the *nuclear starburst* in this paper, the *core starburst* in TB93 involves the whole core of the galaxy, comprising 5 % of the galaxy mass inside $300 - 2000$ pc. As we can see from Fig. 9, the supermassive black hole model leaves room for an efficiency of mass-energy conversion somewhat lower than $f = 0.1$, whereas the nuclear starburst, although it can explain the luminosities of the brightest QSOs, systematically underestimates the density number of QSOs, due to the smallness of its duty cycle. Note that in both cases, there is a remarkable agreement in shape between the predicted and the observed QSO LF at high redshifts. Also the early evolution of the LF is well described by our models. This is illustrated in Fig. 9 by a formal best fit model ($f_{0.1} = 0.3$, $BC_{10} = 1$, and $t_{on,7}^* = 1$) which adjusts the $2 < z < 2.9$ data. In this case, the evolution from $2 < z < 2.9$ to $1.25 < z < 2$ is reproduced. Since we are focusing only on the first inflow episode, which extends only for ~ 3 Gyr, the predictions of our models refer only to the early ($z > 1$) evolution of the QSO luminosity.

Note that the masses of the central black hole or nuclear star cluster produced by the first inflow episode (up to $\approx 10^{10}$ M$_\odot$) are consistent the evidence of Dark Massive Objects (DMOs) in the nuclei of both active and quiescent galaxies (see reviews by Kormendy & Richstone 1995, and van der Marel 1996). So far, the masses are in the range $2 \times 10^6 - 3 \times 10^9$ M$_\odot$, with the largest mass found for M87. There is a correlation of increasing MDO mass with the luminosity of the galaxy, and, since M87 has $M_B = -21.4$, DMOs as massive as 10^{10} M$_\odot$ are expected for $M_B = -24$ galaxies. But such galaxys are very rare, and the corresponding DMOs would be unlikely to be found in the volume of the Universe searched for DMOs until now (M87 is the farthest DMO host, at 15 Mpc). Finally, one important success of our models is that the average MDO-to-galaxy mass ratio of ~ 0.003 (Kormendy & Richstone 1995) is reproduced by the range $\zeta = 0.0015 - 0.005$ of our models.

7 CONCLUSIONS

In this work, we explored the relation between young elliptical galaxies and QSOs within a chemo-dynamical model for evolution of galaxies. In this model, we perform a multi-zone modelling of the chemical enrichment of the gas and stars of a galaxy taking into account the gas flow obtained self-consistently from 1-D hydrodynamical calculations. We were particularly interested in the cooling flow towards the centre of the galaxy, which could feed a QSO hosted in the galactic nucleus.

From a minimal set of assumptions, based on standard one-zone chemical evolution models, our model reproduces the main observational features of elliptical galaxies: 1) the central metallicities of massive galaxies are supersolar; 2) the ratio [Mg/Fe] is supersolar in the core of the galaxy as well as over the whole galaxy; 3) the galaxy shows sizable metallicity gradients; 4) systems with larger masses tend to have larger metallicities, thus reproducing the mass-metallicity relation of elliptical galaxies; 5) elliptical galaxies can be the main responsibles for the ICM iron content: the ICM iron mass per unit luminosity of cluster galaxies ($\sim 10^{-2}$ M$_\odot$/ L$_\odot$) is reproduced.

One very important time scale for the enrichment of the ICM is the time $t_{w,e}$ of the end of early wind phase, during which the gas content in the galaxy is reduced by a factor of ten. $t_{w,e}$ is longer than ~ 1.5 Gyr for normal or bright galaxies. For the iron enrichment, the relevant time scale is even longer, because the Fe-rich gas front arrives at the galaxy edge later than $t_{w,e}$.

From the success of the model in reproducing elliptical galaxies, a number of standard assumptions of the classic one-zone chemical evolution models remain valid when the hydrodynamics is considered: 10^8 yr star formation time scale, Salpeter IMF, stellar yields, $A_{SN\,I} = 0.1$. However, the linear star formation law usually adopted by one-zone models seems to be excluded, since the resulting model would be unrealistic, not reproducing the properties of elliptical galaxies, as seen from the drawbacks of model 2(0): too low central metallicities; too high [Mg/Fe] ratio; the nucleus mass is too small to explain the luminosity of a QSO.

We should take note of two possible discrepancies between the results of our models and the observations: 1) supersolar metallicities are predicted for the hot gas in the galactic halo, while ASCA measurements imply subsolar abundances; 2) we predict a trend of [Mg/Fe] decreasing with galactic mass, which is the opposite of the trend inferred from determinations of metal indices. If these contradictions are real, they could indicate that some of the standard assumptions of the chemical evolution modelling do not apply. We should be aware, however, of the uncertainties in deriving the abundances in the hot galactic halos (besides the dilution by the ICM, which lowers the metallicity in the halo), and of the difficulties in obtaining [Mg/Fe] trends from the observed variation of Mg and Fe line strengths with the galaxy mass.

In addition to the fact that the model satisfy a number of observational constraints on ellipticals, it makes definite predictions about the relation between the evolution of ellipticals and that of QSOs.

A high-metallicity core is rapidly built-up. For the gas, solar metallicities are reached in 10^8 yr for oxygen, and 3×10^8 yr for iron. For the stars, the magnesium abundance becomes solar at 2×10^8 yr and the iron at 8×10^8 yr. In this way, the high abundances derived for high redshift QSOs are reached in a reasonably short time scale. One important application of these results is that the enrichment time scales predicted by our chemo-dynamical model provide a chemical clock which could constrain cosmological scenarios. For instance the ~ 1 Gyr time scale for metal production implies an age at least larger than 1 Gyr for the Universe at $z \sim 5$, since even the more distant QSOs exhibit metals in their spectra. In addition, the short time scales for enrichment both of gas and stars make plausible the starburst model for AGN, which requires a high metallicity core formed early in the evolution of the galaxy.

It is important to note that the luminosity and metallicity of QSOs identified with the central region of the young elliptical are explained with no need for all the galaxy having a global starburst coordinated with the central starburst. In this way, extremely high luminosities ($\sim 10^{15}$ $L_\odot$) are avoided for the proto-QSO. These extreme luminosities, predicted by one-zone models of formation of elliptical galaxies (e.g. model M4 of HF93), have never been detected in high redshift observations. Note that probably only the inner regions of the young galaxy, due to their higher surface brightness, would have star formation detectable at high redshifts. As a matter of fact, deep spectroscopy observations have revealed a population of star-forming galaxies at redshift $3 \lesssim z \lesssim 3.5$, the Lyman break galaxies (LBGs), discovered on the basis of a Lyman limit break superposed on their UV continuum (Steidel et al. 1996; Giavalisco, Steidel & Macchetto 1996). The LBGs show many characteristics expected for primeval galaxies, and, assuming a Salpeter IMF, their inferred SFRs are in the range $4 - 90 h_{50}^{-2}$ $M_\odot$ yr^{-1}, inside a typical half-light radius of $1.8 h_{50}^{-1}$ kpc ($q_0 = 0.5$). These levels of star formation are remarkably close to the typical range of $20 - 50$ $M_\odot$ yr^{-1} for the SFR inside a radius of 1 kpc in the fiducial model. In addition, the LBGs are expected to be the high-redshift counterparts of the present-day spheroidal component of luminous galaxies, since their co-moving density is roughly comparable to that of present-day bright ($L \geq L^*$)galaxies and the widths of the interstellar absorption lines in their spectra imply circular velocities of $170 - 300$ km s^{-1}, typical of the potential well depth of luminous ellipticals. Therefore, for $z \lesssim 3.5$, the observations of ongoing star formation in galaxies seems to rule out the high luminosities predicted by the one-zone models for the progenitors of present-day $\sim L^*$ galaxies.

The luminosities of the one-zone model could still be consistent with the observations of LBGs, if there is dust absorbing the blue and UV light and re-emitting it in the far-IR/sub-mm. However, comparisons between the observed colours of LBGs and those predicted by spectral synthesis models (Pettini et al. 1998) indicate only modest dust attenuation (an extinction at 1500 Å between lower and upper limits of ~ 2 and ~ 6), and, therefore, dust absorption is unable to hide the high luminosities of the one-zone model. In addition, in view of the evidence that the LGBs are the progenitors of the present-day luminous ($\sim L^*$ or brighter) galaxies, rather than sub-units being assembled into a larger system, it seems that the LBGs are allowing us to witness one stage in a single event of formation of a massive galaxy, with the global star formation proceeding, however, at a milder rate than in the one-zone model. In the end, the main reason why the one-zone model overpredicts the luminosity is that it overproduces metals. The model M4 of HF93 predicts ~ 10 times the solar metallicity over the whole galaxy. The observations, however, allow this extremely high metallicity only at the very nucleus of the galaxy, at most. Over an effective radius, the metallicity of a giant elliptical is roughly solar. These metallicities are correctly predicted by our multi-zone model (see the values of $\langle$[Mg/H]$\rangle_{10}$ and $\langle$[Fe/H]$\rangle_{10}$ in Table 3). Moreover, assuming that the observed negative metallicity gradients continue beyond the effective radius, the mass-averaged metallicity would be subsolar over the whole galaxy. Therefore, scaling the metals produced in the one-zone approximation to amounts consistent with the observations, brings down the predicted luminosities by about one order of magnitude.

All our models predict a massive central (through the inner 100 pc) cooling flow during the first 1-2 Gyr of the galaxy evolution. Within the scenario in which the luminosity of the galactic nucleus is fed by the central inflow, for a reasonable epoch of formation of the spheroidal systems, the epoch of building-up of the nucleus by the central inflow coincides with the maximum in QSO activity ($2 < z < 3$). Also the decrease of the central inflow rate for $t > 1$ Gyr is consistent with the decline of luminosity inferred for $z < 2$ from the evolution of QSO LF with redshift.

One of our models exhibits recurrent late central cooling flow episodes, which are brief (a few 10^7 yr) and involve decreasing amounts of mass. The gas inflow into the inner 100 pc is regulated by episodes of star formation leading naturally to several short episodes of central inflow, thus giving support to the episodic scenario for evolution of the LF of QSOs.

The model also explains the luminosities of QSOs. The central cooling flow rates explain bolometric luminosities of up to 10^{47} erg s^{-1}, for an efficiency f of mass-energy conversion of 0.1. However, the bolometric luminosities of the brightest QSOs ($\approx 10^{48}$ erg s^{-1}) cannot be explained by a continuous deposition of the central inflow. Rather, the highest QSO luminosities require a discrete deposition, in which the gas is accumulated during ≈ 1 Gyr and then consumed by a central engine in few 10^7 yr. Accordingly, we have made some predictions on the QSO LF at $z \gtrsim 1$ based on a simple discontinuous model for QSO activity, in which there is two short gas consumption events during the first central inflow episode. We scaled the QSO LF to the present day elliptical LF, assuming that all ellipticals have harboured a QSO during their evolution. Both the starburst and the supermassive black hole models predict the right shape of the QSO LF, but the nuclear starburst systematically underestimates the density number of QSOs. In addition, our model reproduces the evolution of the LF between $z = 1.25$ and $z = 2.9$. In our models, the mass deposited by the first central inflow represents 0.15-0.5 % of the present day luminous mass of the galaxy. Assuming that this mass goes to the formation of a central object (star cluster or black hole), the model correctly predicts for the Dark Massive Objects (DMOs) in the nuclei of galaxies, both the masses and the DMO-to-galaxy mass ratios.

Another conclusion derived from our models is that the hosts of high-redshift AGN should be relatively mature objects. The calculated evolution of the inner cooling flow and energetic considerations imply that the gas deposited by the inflow in the nucleus should accumulate during ~ 1 Gyr before triggering a short-lived AGN activity event. On the other hand, except for extremely large galaxies (present-day $M_B = -24$), the first, massive cooling flow, responsible for maintaining the AGN activity, lasts for $2 - 3$ Gyr. In this scenario, if the high redshift galaxy is to display strong AGN activity, its probable age would range from ~ 1 to ~ 3 Gyrs. The minimum age of ~ 1 Gyr for QSO hosts derived above is consistent with the ~ 1 Gyr time scale for metal enrichment, needed to explain the strong metal lines observed even in $z \sim 5$ QSOs.

One further prediction of our models is that, at the present, only the most massive objects should be host to powerful AGN, but at high redshift powerful AGN activity is expected even for hosts of smaller mass. Interestingly enough, this is what seems to be observed, for radio galaxies at least. Models 1 and 2 are examples of sub-L^* galaxies with strong AGN activity at high redshift. Note that ζ increases with decreasing galaxy mass for masses below $M_G \approx 10^{12}$ M$_\odot$. Since this parameter describes the relative importance of the first cooling flow episode occuring when the galaxy is less than $2 - 3$ old, this means that for the lower mass systems, the efficiency of building-up the nucleus is higher than in larger systems, and that they have an early cooling flow massive enough to sustain a strong AGN activity. However, this activity is limited only to the 2-3 first Gyr of the galaxy and, therefore, smaller systems with strong nuclear activity are to be found only at high redshift. Even in the case of the episodic scenario of model 2(1/3), the late nuclear activity is much weaker at low redshift (in this model, the two late central inflow episodes deposit only 1.8 % and 1 % of the mass of the first inflow episode). On the other hand, models 10, 20 and 50 exhibit a present-day massive central cooling flow which could trigger AGN activity. In these massive systems, the late cooling flow may accumulate into the nucleus an amount of mass comparable to that of the early cooling flow (model 20 is typical of this case, the late cooling flow deposits 1.65×10^9 M$_\odot$, i.e. 47 % of the mass of the first cooling flow). Only these objects, therefore, would harbour, intense AGN activity at low redshift. Support to this picture is given by recent analysis of host galaxies of powerful nearby ($z \lesssim 0.3$) AGN, belonging to three samples — radio galaxies radio-loud quasars, and radio-quiet quasars (Taylor et al. 1996). For all three classes of AGN, the host galaxies are large (half-light radius $r_{1/2} \geq 10$ kpc) and luminous (K-band luminosity $L_K \geq L^*$). (Note that the less massive model exhibiting a present-day central is model 10, with $M_B = -21.8$, or $L_B = 2L^*$.)

Finally, we should note that, although pure luminosity evolution seems to reproduce the evolution of the QSO LF, in our models the individual QSOs do not dim over cosmological time scales, but rather are short-lived (i.e., $t_{on} = 1 - 3 \times 10^7$ yr). In order to comply with the energetic requirements of the QSOs, their activity must occur in short episodes of massive consumption of mass accumulated in the galactic nucleus during a much longer span of time (~ 1 Gyr). This sort of episodic activity displayed by our model for QSOs seems to be a rule among the AGN in general, since for other class of AGN, the radio galaxies, the radio LF also seems to follow pure luminosity evolution, and yet the radio sources themselves seem to have lifetimes of only a few 10^7 yr. As a matter of fact, a comparison between the properties of the radio-loud population and the present model would be very useful to clarify the relation of the QSO phenomenon and the early evolution of elliptical galaxies, since radio observations allow us to explore the $z > 2$ domain without the need of uncertain corrections for dust absorption and lensing bias that hamper the optical tecniques.

ACKNOWLEDGMENTS

A.C.S.F. acknowledges support from the Brazilian agency CNPq. We thank the referee James Dunlop for a number of suggestions which helped us to improve this paper significantly and specially for the remarks on the radio loud population discussed in the two last paragraphs of this paper.

REFERENCES

Andreani P., La Franca F., Cristiani S., 1993, MNRAS, 261, L35
Aretxaga I., Boyle B.J., Terlevich R.J., MNRAS, 275, L27
Arimoto N., Yoshii Y., 1987, A&A 173, 23
Arnett D. W., 1991, in Lambert D.L., ed., Frontiers of Stellar Evolution, ASP Conf. Ser. 20. ASP, San Francisco, p. 389
Awaki H., et al., 1994, PASJ, 46, L45

Bahcall J.N., Kirkakos S., Schneider D.P., 1996, ApJ, 457, 557
Bower R.G., Lucey J.R., Ellis R.S., 1992, MNRAS, 254, 589
Boyle B.J., Terlevich R.J., 1998, MNRAS, 293, L49
Boyle B.J., Shanks T., Peterson B.A., 1988, MNRAS, 235, 935
Boyle B.J., Jones L.R., Shanks T., Marano B., Zitelli V., Zamorani G., 1991, in Crampton D., ed., The Space Distribution of Quasars, ASP Conf. 21. ASP, San Francisco, p. 191
Bruzual G., Charlot S., 1993, ApJ, 405, 538
Burkert A., Hensler G., 1989, in Beckman J.E., Pagel B.E.J., eds., Evolutionary Phenomena in Galaxies. CUP, Cambridge, p. 230
Burkert A., Truran J.W., Hensler G., 1992, ApJ, 391, 651
Capellaro E., Turatto M., Tsvetkov D.Yu., Bartunov O.S., Makarova I.N., 1993, A&A, 273, 383
Carollo C.M., Danziger I.J., Buson L., 1993, MNRAS, 265, 553
Caughlan G.R., Fowler W.A., 1988, Atomic Data & Nuclear Data Tables, 40, 283
Cavaliere A., Padovani P., 1988, ApJ, 333, L33
Ciotti L., D'Ercole A., Pellegrini S., Renzini A., 1991, ApJ, 376, 380
David L. P., Forman W., Jones C., 1990, ApJ, 359, 29
David L. P., Forman W., Jones C., 1991, ApJ, 369, 121
Davies R.L., Sadler E.M., Peletier R.F., 1993, MNRAS, 262, 650
Disney M.J. et al., 1995, Nat, 376, 150
Elbaz D., Arnaud M., Vangioni-Flam E., 1995, A&A, 303, 345
Fabian A.C., Arnaud K.A., Bautz M.W., Tawara Y., 1994, ApJ, 436, L63
Fisher D., Franx M., Illigworth G., 1995, ApJ, 448, 119
Forman W., Jones C., David L., Franx M., Makishima K., Ohashi T., 1993, ApJ, 418, L55
Forman W., Jones C., Tucker W., 1994, ApJ, 429, 77
Friaça A. C. F., 1986, A&A, 164, 6
Friaça A. C. S., 1990, in Ferrini F., Franco J., Matteucci F., eds, Chemical and Dynamical Evolution of Galaxies. ETS, Pisa, p.561
Friaça A. C. F., 1993, A&A, 269, 145
Friaça A.C.S, Terlevich R.J., 1994, in Tenorio-Tagle G., ed., Violent Star Formation from 30 Doradus to QSOs. CUP, Cambridge, p.424
Giavalisco M., Steidel C.C., Macchetto F.D., 1996, ApJ, 470, 189
Gorgas J., Efstathiou G., Salamanca A., 1990, MNRAS, 245, 217
Greggio L. , Renzini, A., 1983, A&A, 118, 217
Grevesse N., Anders E., 1989, in Waddington C.J., ed., Cosmic Abundances of Matter. AIP, New York, p.183
Gruenwald R.B., Viegas S.M., 1992, ApJS, 78, 153
Güsten R., Mezger P.G., 1983, Vistas Astron., 26, 159
Hamann. F., Ferland G., 1992, ApJ, 391, L53
Hamann. F., Ferland G., 1993, ApJ, 418, 11
Haehnelt M.G., Rees M.J., 1993, MNRAS, 263, 161
Heckman T.M., Armus L., Miley G.K., 1987, AJ, 92, 276
Hillebrandt W., 1982, A&A 110, L3
Hutchings J.B., Janson T., Neff S.G., 1989, ApJ, 342, 660
Hutchings J.B., Holtzman J., Sparks W.B., Morris S.C., Hanish R.J., Mo J., 1994, ApJ, 429, L1
Hutchings J.B., Morris S.C., 1995, AJ, 109, 1541
Iben I. Jr., Renzini A., 1983, ARAA, 21, 271
Isaak K.G., MaMahon R.G., Hills R.E., Withington S., 1994, MNRAS, 269, L28
Kennicutt, R.C., Jr., 1989, ApJ, 344, 685
Kormendy J., Richstone D., 1995, ARAA, 33, 581
Larson R.B., 1974a, MNRAS, 166, 585
Larson R.B., 1974b, MNRAS, 169, 229
Liedahl D.A., Osterheld A.L., Goldstein W.H., 1995, ApJ, 438, L115
Lowenstein M, et al., 1994, ApJ, 436, L75
McLeod K.K., Rieke G.H., ApJ, 454, L77
McMahon R.G., Omont A., Bergeron J., Kreysa E., Haslam C.G.T., 1994, MNRAS, 267, L9
Matsushita K., et al., 1994, ApJ, 436, L41
Matteucci F., 1992, ApJ, 397, 32
Matteucci F., 1994, A&A, 288, 57
Matteucci F., Tornambè A., 1987, A&A, 185, 51
Matteucci F., Padovani P., 1993, ApJ, 419, 485
Negroponte J., White S.D.M., 1983, MNRAS, 205, 1009
Nomoto, K., Thielemann K. F., Yokoi K., 1984, ApJ, 286, 644
Omont A., McMahon R.G., Cox P., Kreysa E., Bergeron J., Pojot F., Storrie-Lombardi L.J., 1996, A&A, 315, 1
Padovani P., Matteucci F., 1993, ApJ, 416, 26
Pettini M., Steidel C.C., Adelberger K.L., Kellogg M. Dickinson M., Giavalisco M., 1998, in Shull J.M., Woodward C.E., Thronson H, eds., ORIGINS. ASP Conf. Ser., in press
Renzini A., Voli M., 1981, A&A, 94, 175
Renzini A., Buzzoni A., 1986, in Chiosi, C., Renzini, A., eds, Spectral Evolution of Galaxies. Reidel, Dordrecht, p. 195
Renzini A., Ciotti L., 1993, ApJ, 416, L49
Richtmyer R.D., Morton K.W., 1967, Difference Methods for Initial Value Problems. Interscience, New York.
Ronnback J., van Groningen E., Wanders I., Orndahl E., 1996, MNRAS, 283, 282
Samland M., Hensler G., Theis Ch., 1997, ApJ, 476, 544
Sarazin C.L., White R.E., III, 1987, ApJ, 320, 32
Serlemitsos P.J., Lowenstein M., Mushotzky R.F., Marshall F.E., Petre R., 1993, ApJ 413, 518
Schmidt M., 1959, ApJ, 129, 243
—, 1963, ApJ, 137, 758
Schmidt M., Schneider D.P., Gunn J.E., 1991, in Crampton D., ed., The Space Distribution of Quasars, ASP Conf. Ser. 21. ASP, San Francisco, p. 109
Smith E.P., Heckman T.M., Bothun G.D., Romanishin W., Balick B., 1986, ApJ, 306, 64
Smith R.M., Driver S.P., Phillipps S., 1997, MNRAS, 287, 415
Steidel C.C., Giavalisco M., Pettini M., Dickinson M., Adelberger K.L., 1996, ApJ, 462, L17
Talbot R.J., Arnett W.D., 1973, ApJ, 186, 51
Tammann G., 1982, in Rees M., Stoneham R., eds, Supernovae: A Survey of Current Research. Reidel, Dordrecht, p. 371
Taylor G.L., Dunlop J.S., Hughes D.H., Robson E.I., 1996, MNRAS, 283, 930
Terlevich R. J., 1992, in FillipenkoA.V., ed., Relationship between Active Galactic Nuclei and Starburst Galaxies, ASP Conf. 31. ASP, San Francisco, p. 133
Terlevich R. J., 1994, in Tenorio-Tagle G., ed., Violent Star Formation from 30 Doradus to QSOs. CUP, Cambridge
Terlevich R. J., Boyle B. J., 1993, MNRAS, 262, 491
Theis Ch., Burkert A., Hensler G., 1992, A&A, 265, 465
Tinsley B.M., 1980, Fund. Cos. Phys., 5, 287
Tscharnuter W.M., Winkler K.H., 1979, Comp. Phys. Comm., 18, 171
van den Bergh S., McClure R.D., 1994, ApJ, 245, 205
van den Bergh S., Tammann G., 1991, ARA&A, 29, 363
Van der Marel, 1996, in Bender R., Davies R.L., eds., New Light on Galactic Evolution, IAU Symp. 171. Kluwer, Heidelberg, p. 117.
Warren, S.J., Hewett P.C., Osmer P.S., 1994, ApJ, 421, 412
Weaver, T.A., Woosley, S.E., 1993, Phys. Rept., 227, 65
Weiss A., Peletier R., Matteucci F.,1995, A&A, 296, 73
Whelan J., Iben I., Jr., 1973, ApJ, 186, 1007
Woosley, S.E., Weaver, T.A., 1986, in Mihalas D., Winkler K.H., eds, IAU Symposium 89, Radiation Hydrodynamics in Stars and Compact Objects. Springer, Berlin, p. 91
Woosley, S.E., Weaver, T.A., 1995, ApJS, 101, 181
Worthey G., Faber S.M., González J.J., 1992, ApJ, 398, 69

This paper has been produced using the Royal Astronomical Society/Blackwell Science LaTeX style file.

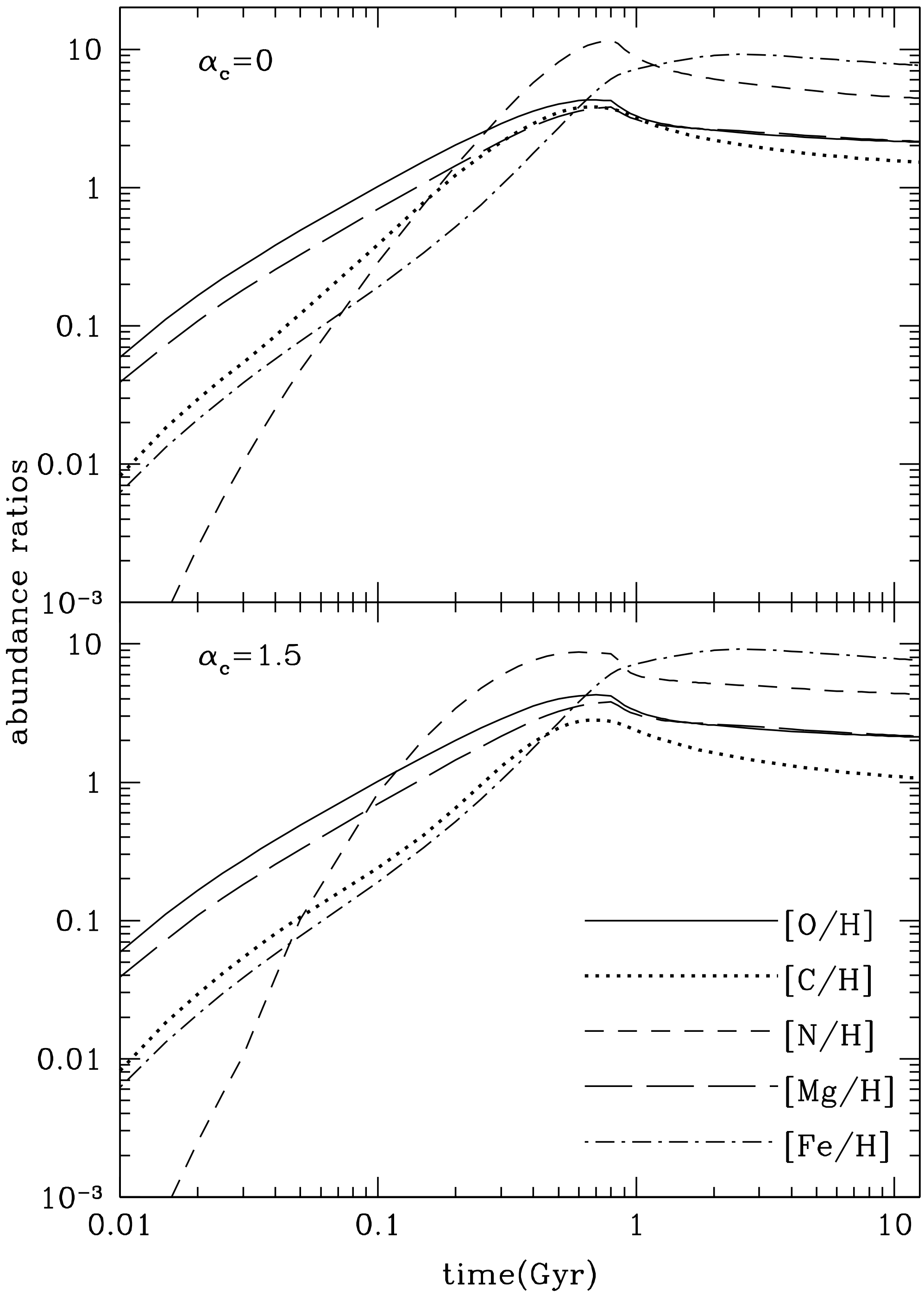

$\alpha_c=0$
$\alpha_c=1.5$
abundance ratios
time(Gyr)
10
1
0.1
0.01
10^{-3}
0.01
0.1
1
10
[O/H]
[C/H]
[N/H]
[Mg/H]
[Fe/H]

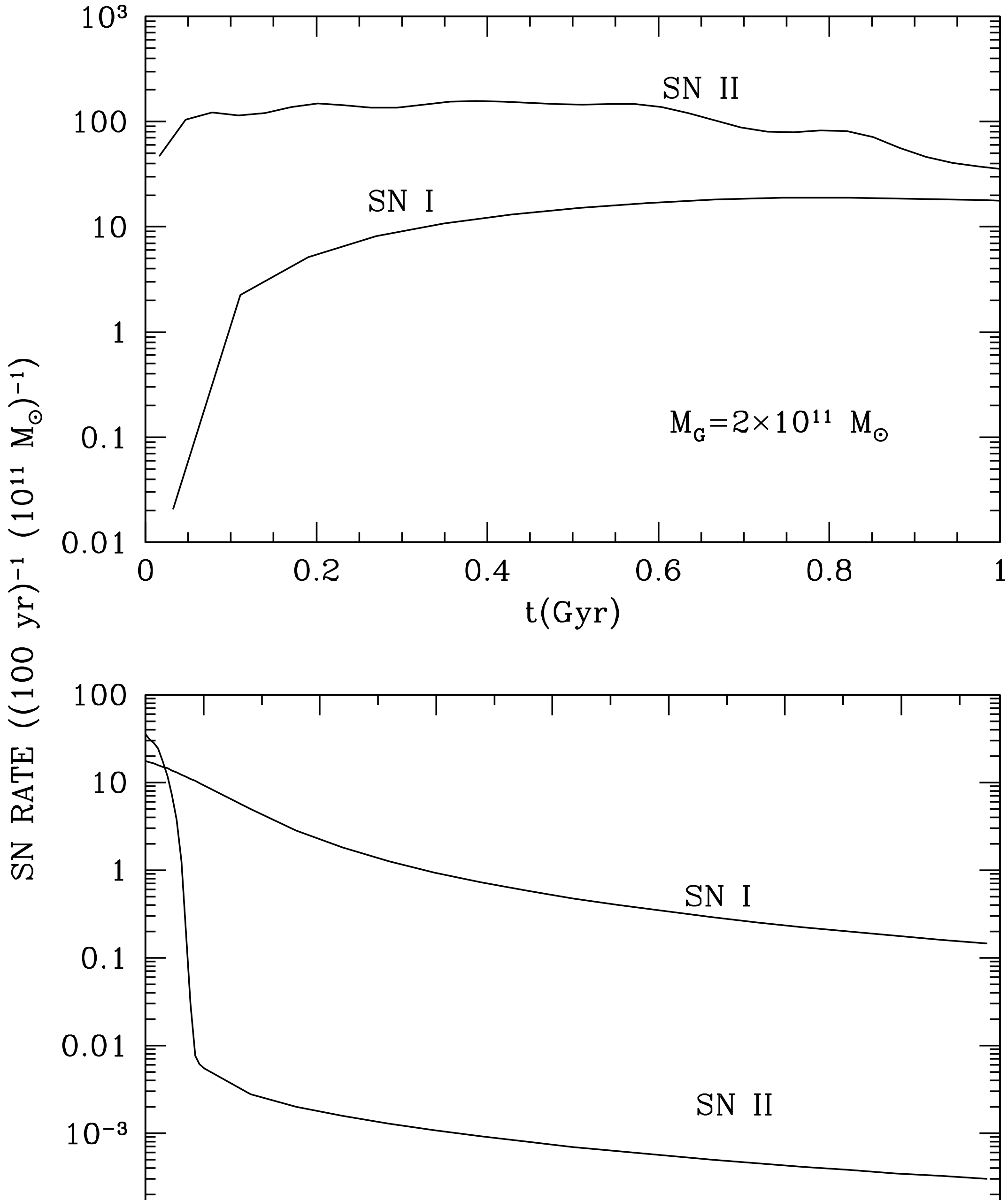

SN II
SN I
$M_G = 2\times10^{11}\ M_\odot$
SN RATE ((100 yr)$^{-1}$ (10^{11} $M_\odot$)$^{-1}$)
t(Gyr)
SN I
SN II
t(Gyr)

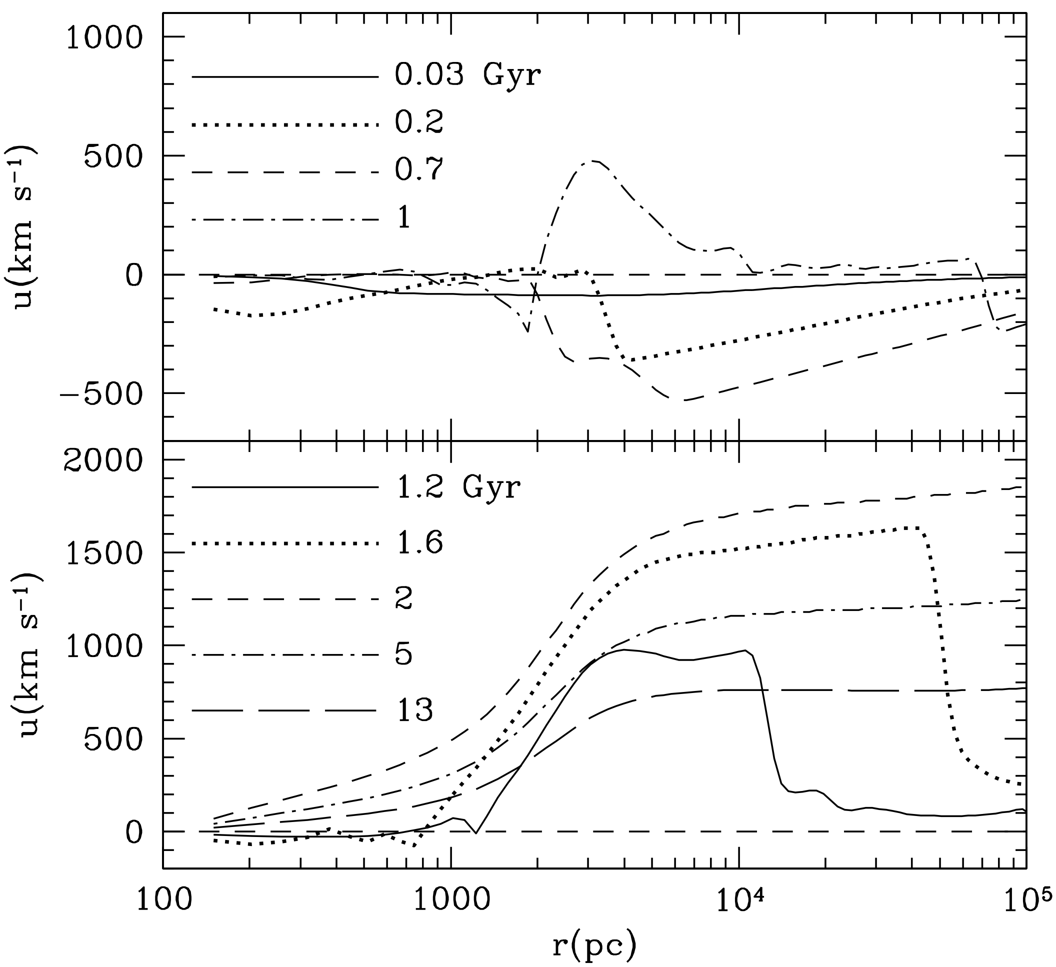

1000
500
0
−500
2000
1500
1000
500
0
u(km s⁻¹)
u(km s⁻¹)
0.03 Gyr
0.2
0.7
1
1.2 Gyr
1.6
2
5
13
100
1000
10⁴
10⁵
r(pc)

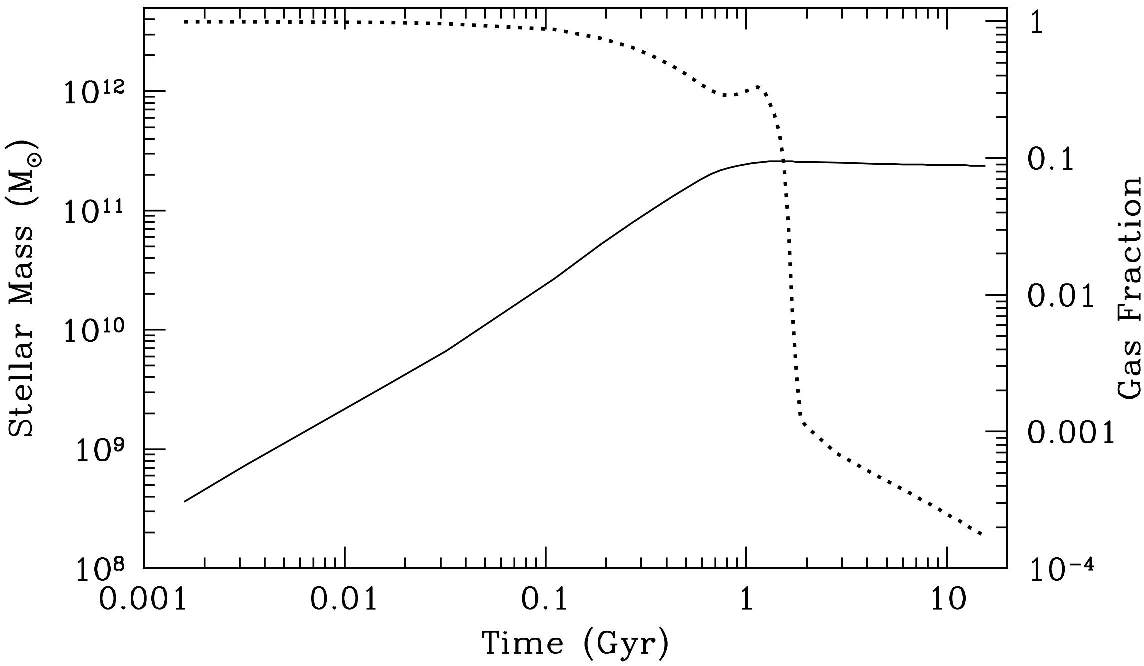

Stellar Mass ($M_\odot$)
Gas Fraction
Time (Gyr)
10^{12}
10^{11}
10^{10}
10^{9}
10^{8}
1
0.1
0.01
0.001
10^{-4}
0.001
0.01
0.1
1
10

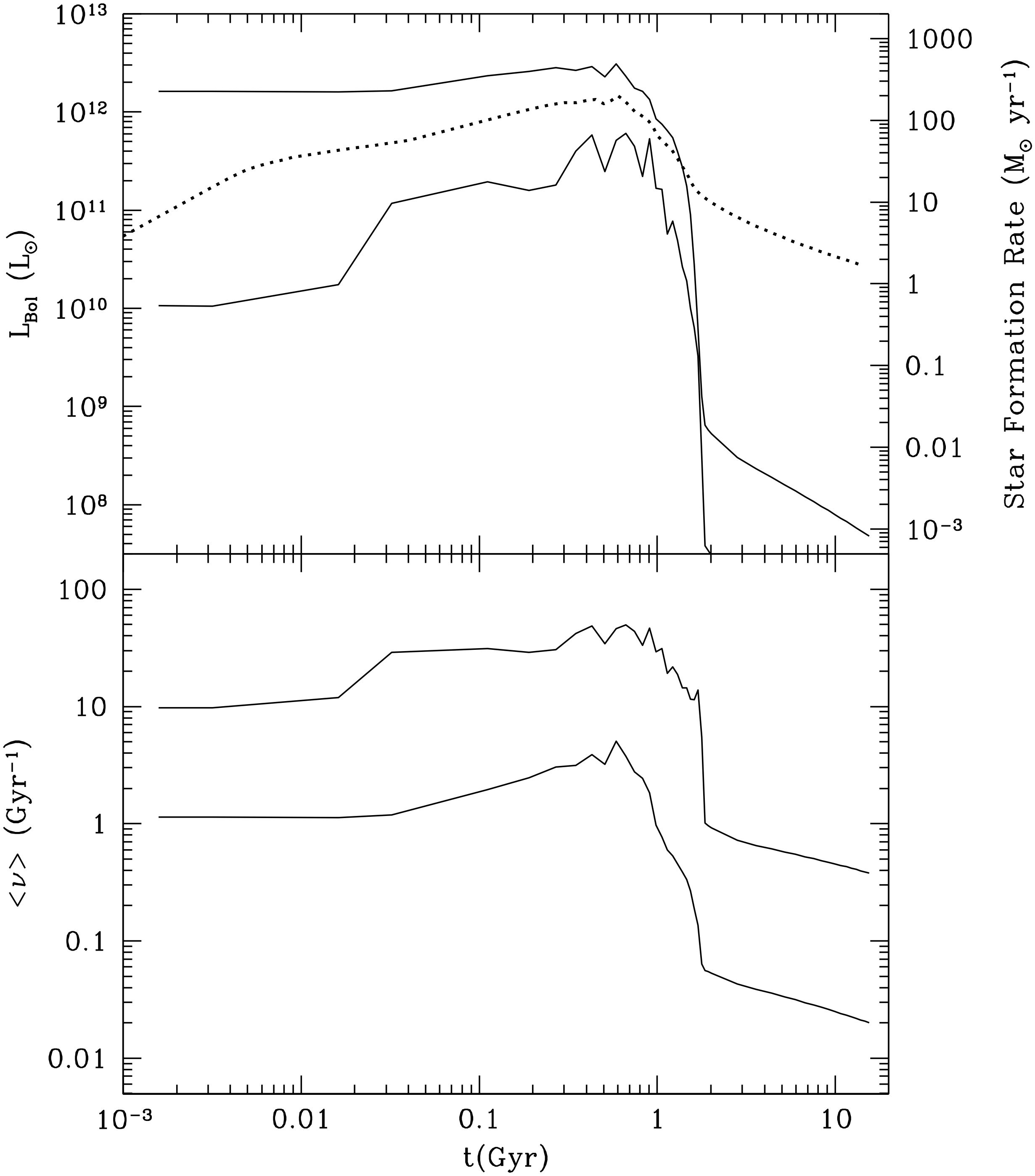

10^{13}
10^{12}
10^{11}
10^{10}
10^{9}
10^{8}
L_{Bol} ($L_\odot$)
1000
100
10
1
0.1
0.01
10^{-3}
Star Formation Rate ($M_\odot$ yr^{-1})
100
10
1
0.1
0.01
$\langle \nu \rangle$ (Gyr^{-1})
10^{-3}
0.01
0.1
1
10
t(Gyr)

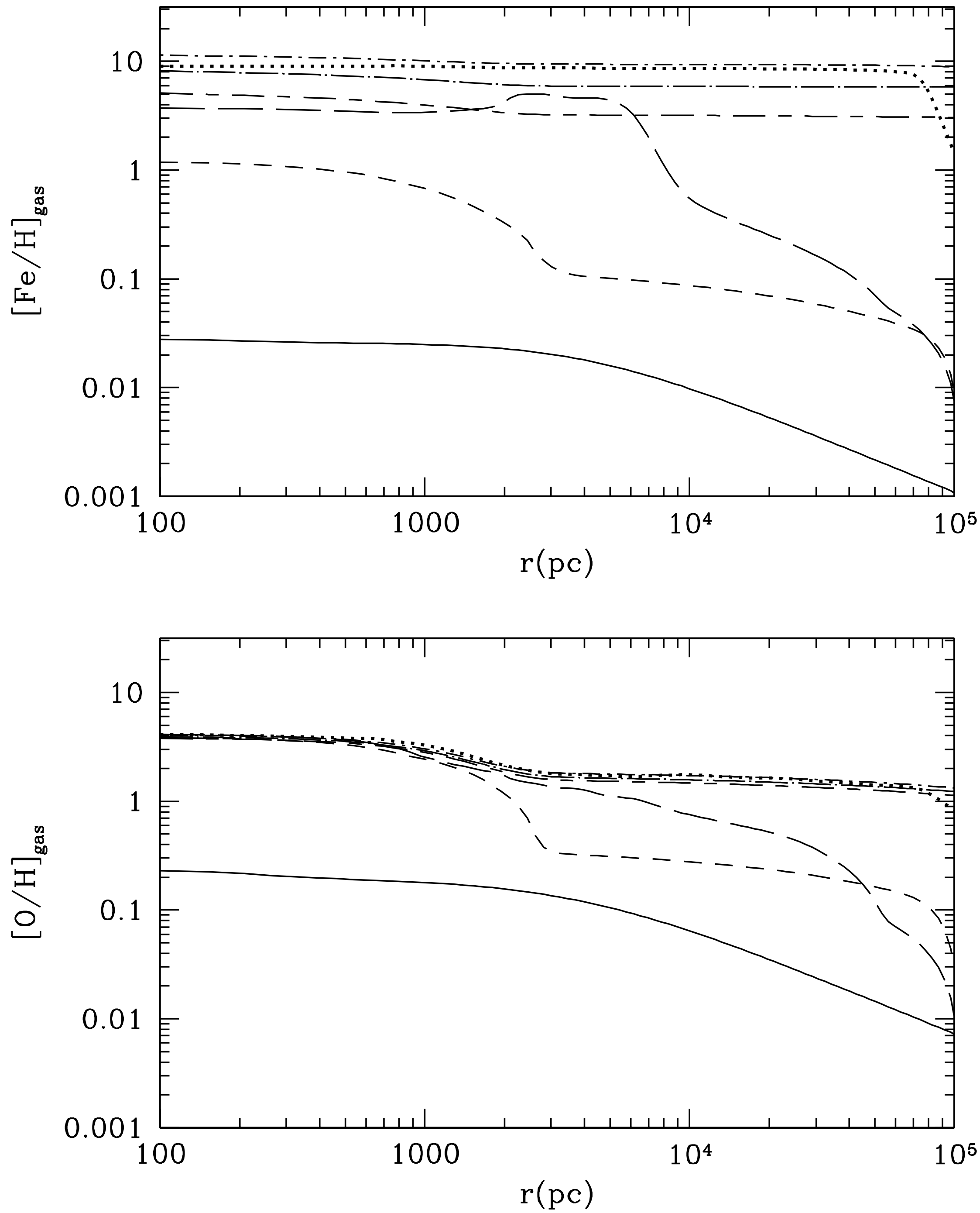
[Fe/H]gas
0.001
0.01
0.1
1
10
100
1000
10⁴
10⁵
r(pc)
[O/H]gas
0.001
0.01
0.1
1
10
100
1000
10⁴
10⁵
r(pc)

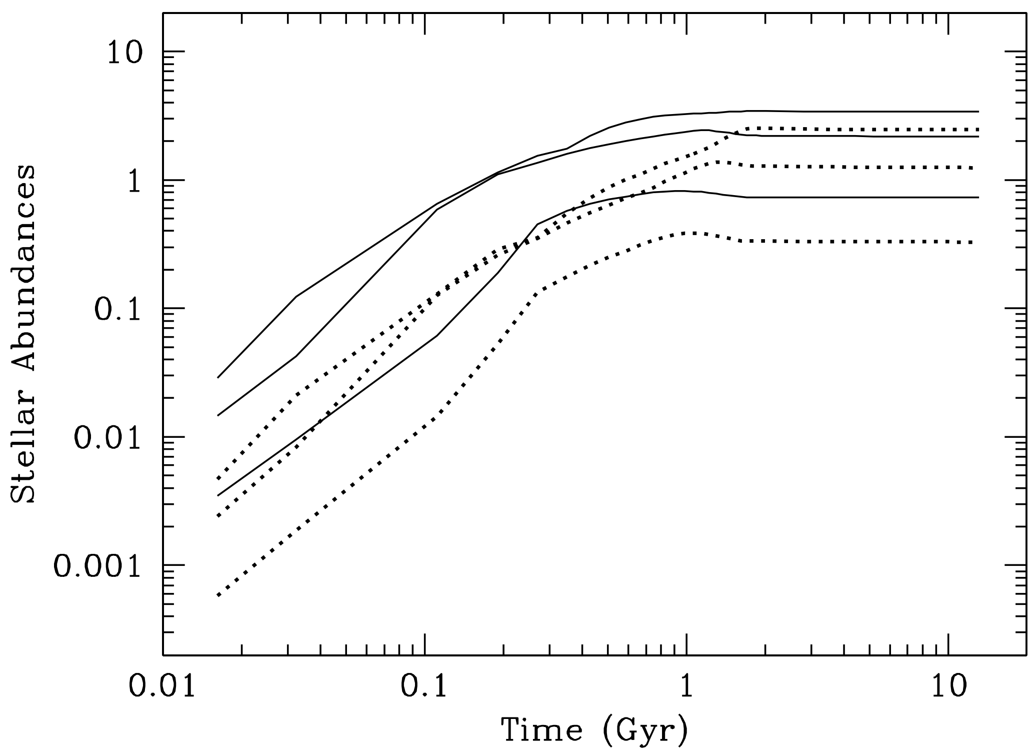

Stellar Abundances
10
1
0.1
0.01
0.001
0.01
0.1
1
10
Time (Gyr)

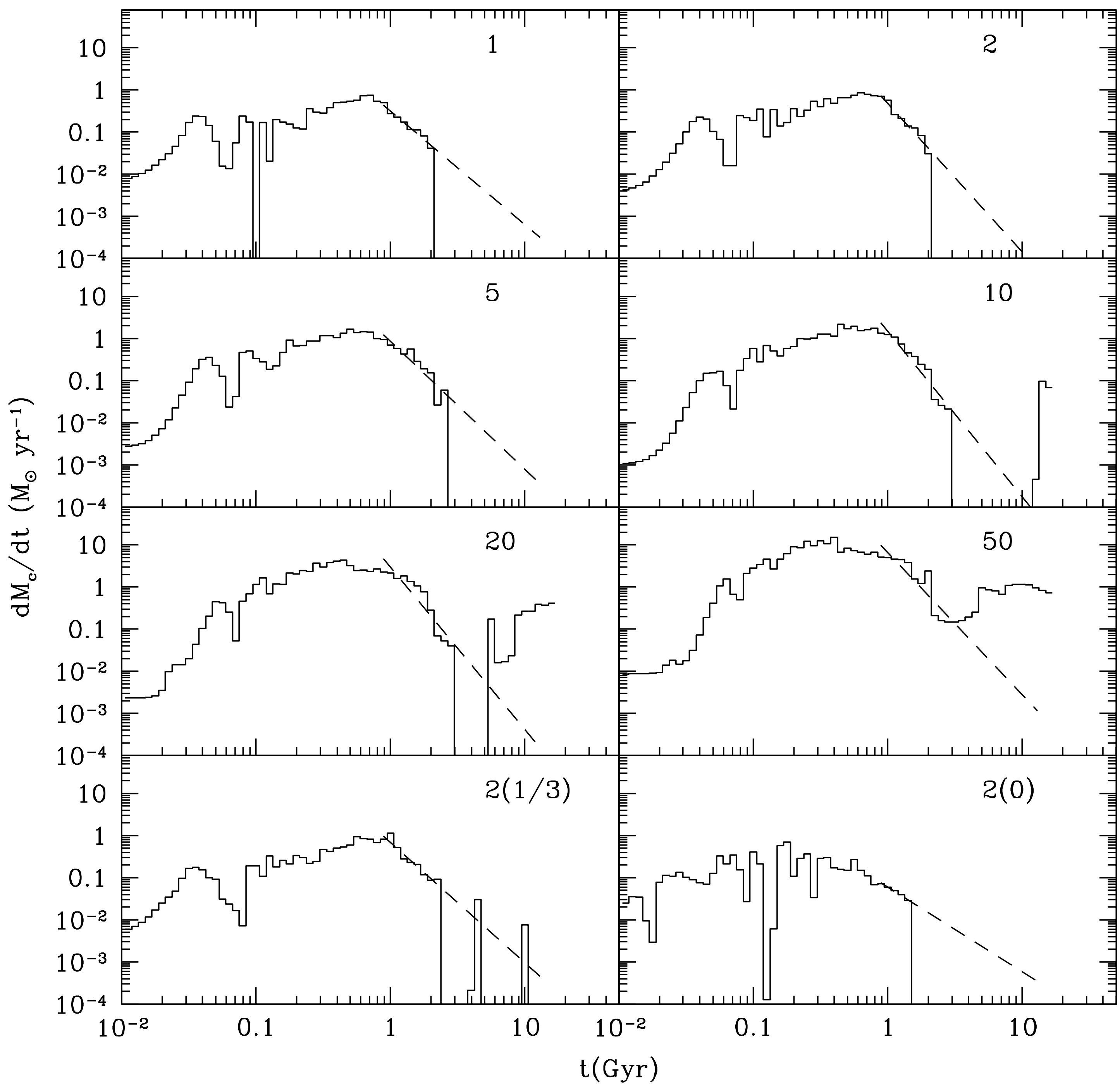

1
2
5
10
20
50
2(1/3)
2(0)
10
1
0.1
10^{-2}
10^{-3}
10^{-4}
0.1
10
t(Gyr)
dM_c/dt ($M_\odot$ yr^{-1})

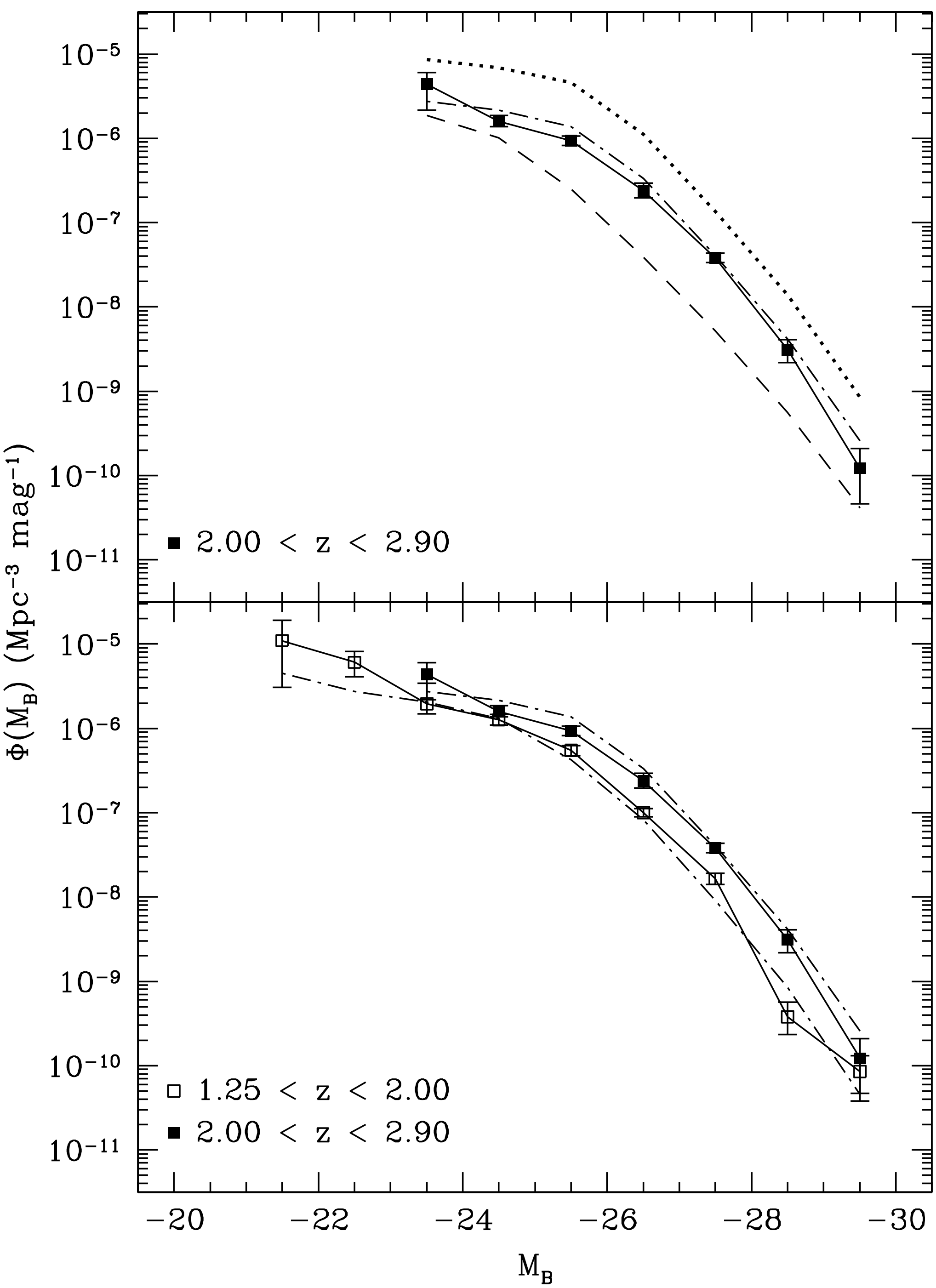

$\Phi(M_B)$ (Mpc^{-3} mag^{-1})
10^{-5}
10^{-6}
10^{-7}
10^{-8}
10^{-9}
10^{-10}
10^{-11}
2.00 < z < 2.90
1.25 < z < 2.00
2.00 < z < 2.90
−20
−22
−24
−26
−28
−30
M_B